國立台灣大學理學院物理學系

碩士論文

Department of Physics

College of Science

National Taiwan University

Master Thesis

光控制自聚性矽/鍺量子點在光電元件上的應用
Light-Controlled Self-Assembly of Ge/Si Quantum Dots for
Optoelectronic Devices

黃少聰
Shao-tsung Huang

指導教授：汪治平 博士
共同指導教授：陳賜原 博士
Advisor: Jyhpyng Wang, Ph.D.
Co-Advisor: Szu-yuan Chen, Ph.D.

中華民國 103 年 7 月
July, 2014

國立臺灣大學碩士學位論文
口試委員會審定書

光控制自聚性矽/鍺量子點在光電元件上的應用
Lght-Controlled Self-Assembly of Ge/Si Quantum Dots for Optoelectronic Devices

本論文係黃少聰君（R00222029）在國立臺灣大學物理學系、所完成之碩士學位論文，於民國 102 年 07 月 29 日承下列考試委員審查通過及口試及格，特此證明

口試委員：

_____ （簽名）

（指導教授）

陳賜厚　　　　　　　　李勝偉

_____

_____

_____

i

誌謝

摘要

自聚性鍺/矽量子點 (self-assembled Ge/Si quantum dots) 的研究在 1990 年晚期才開始進行。當量子點小於 10 奈米 (nm) 時，量子點內量子侷限 (quantum confinement) 的效應會讓量子點能隙 (band gap) 吸收波段 (absorption wavelength) 改變。因此，透過控制鍺/矽量子點的大小，鍺/矽量子點應用在光度感應器 (photodetector)、LED 與太陽能電池 (solar cell) 這幾種光電元件上有著頗有潛力的發展。

在我們的研究中，我們用脈衝雷射沉積 (pulsed laser deposition, PLD) 的方式，在攝氏 400 度的矽基板 (100) 上成長 2 Å 的鍺。在此厚度下，矽與鍺之間 4.2% 晶格大小不匹配 (lattice mismatch) 所造成的應力 (strain) 不夠大，無法以斯特蘭斯基—克拉斯坦諾夫成長 (Stranski–Krastanow growth,S-K growth) 的方式形成量子點，因此我們在此厚度 (2 Å) 下沒有看到量子點。然而，在此樣品上，使用波長為 355 奈米的脈衝雷射光照射後，我們觀察到了量子點的形成，我們觀察到最小的量子點大小為平均直徑 13.3 奈米，同時，也達成了密度為 1.6×10^{11} cm^{-2} 的量子點。

實驗結果指出，透過改變鍺的厚度跟打在基板上雷射的能量，能夠控制鍺量子點在矽基板上形成的大小。在製造更佳效能的光電元件上有著不錯的潛力。

關鍵字： 鍺/矽量子點, 脈衝雷射沉積, PLD, 斯特蘭斯基—克拉斯坦諾夫成長, S-K 成長, 雷射激發表面結構

Abstract

It was only in the late 1990s did the research of germanium on silicon self-assembled quantum dots (QDs) begin. Due to the effect of quantum confinement in the quantum dots with dot size less than 10 nm, the absorption wavelength of the energy bandgap shifts. Therefore, by controlling the size distribution of Ge/Si QDs, there is big potential for the application in optoelectronic devices such as photodetectors, LEDs, and solar cells.

In our experiments, thin film of germanium with thickness of 2 Å was grown on silicon (100) by pulsed laser deposition (PLD) with 400°C substrate temperature. With such small thickness (2 Å), the strain due to 4.2% lattice mismatch between germanium and silicon is not enough for the Stranski–Krastanow(S-K) growth of QDs. As a result, no QDs were observed. However, after the irradiation of the sample with 355-nm pulsed laser beam, the formation of QDs was observed. The smallest average quantum dot diameter observed was about 17 nm and the density of dots was 1.6×10^{11} cm^{-2}.
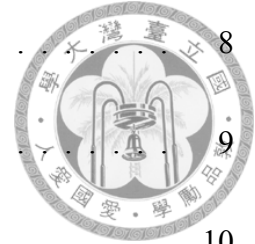
The results indicate that by varying different parameters such as the thickness of germanium thin film and the fluence of the laser beam irradiated on the sample, one can control the size of the Ge QDs formed on Si substrate. This technique provides control over QDs size, which in result provides a new route for the fabrication of the optoelectronic devices with better performances.

Keywords: Ge/Si quantum dots, pulsed laser deposition, PLD, Stranski-Krastanow growth, S-K growth, laser-induced surface structure

Contents

List of Figures

Chapter 1

Inroduction

1.1 Quantum Dots

Quantum Dots (QDs) are semiconductor particles which are very small in size of the scale in nanometers. When the size reaches this scale, the electrons or holes feel a strong confining potential, and their energy become discrete.
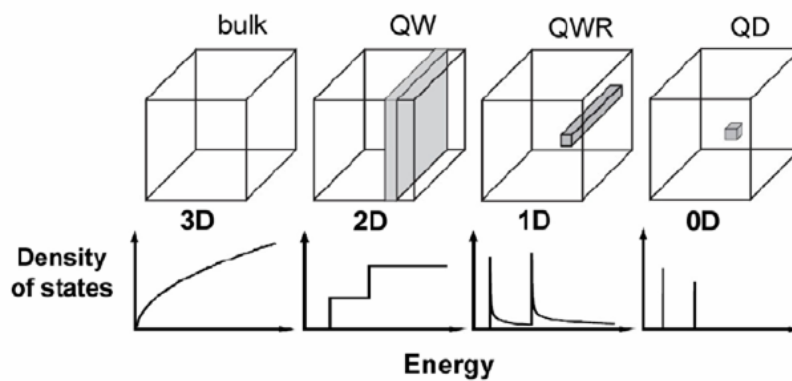
Figure 1.1: Schematic graph of the quantum nano-structures and their density of states.

Figure 1.1 shows the schematic graph and the density of states of bulk, quantum wells, quantum wires, and quantum dots [1]. The electrons can move freely in three directions in bulk materials. In the quantum wells, they are confined to move in two directions, and one direction in the quantum wires. In the quantum dots, all three directions are con-

fined. This confinement results in the quantization of the electron energy and the variation of the density of states. The energy levels in the quantum dots are similar to the wavefunction of an atom. Therefore, quantum dots are also called the large 'artificial atoms.' The word 'large' is due to the energy quantization in the crystals containing as many as 10^4 atoms. [2]
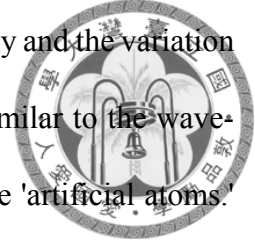
There are several materials of quantum dots. For example, Ge/Si [3], InAs/GaAs [4], MgO/SrTiO$_3$ [5], and etc. In our research, we focused on Ge/Si quantum dots.

1.2 Growth of the Ge/Si(100) Quantum Dots

The growth of Ge/Si(100) quantum dots can be described with a model system for studying the growth dynamics of the Stranski-Krastanov (S-K) mode.
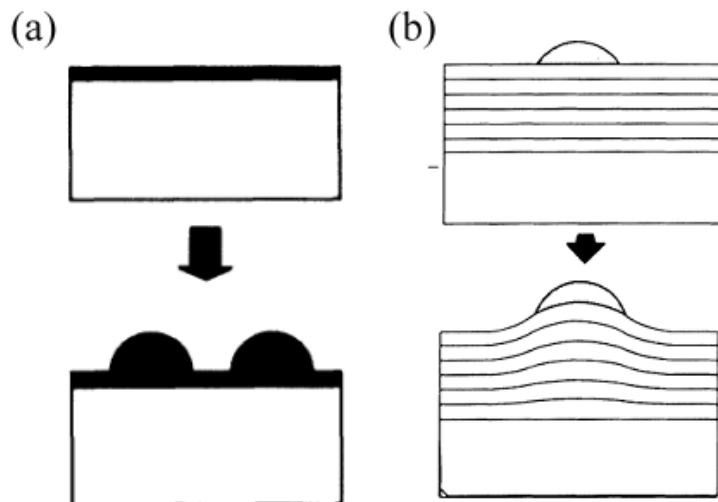
Figure 1.2: Schematic graph of the S-K mode in different conditions. (a) Strain relaxation due to the lattice mismatch when the film thickness reaches a critical value. (b) Strain relaxation form the local elastic deformation of near surface layers.)

In the beginning, the germanium film starts to be grown on the silicon(100) substrate to form wetting layer where the germanium film lattice constant adapts to that of the silicon

substrate. After several layers, due to the 4.2% lattice mismatch between the silicon sub-strate and the germanium film, there is an elastic strain, which increases linearly with the increase of the thickness of the germanium film. When the film thickness of germanium exceeds an critical value, elastic strain relaxation occurs in nucleating dots. This process is the transition from two-dimensional growth of wetting layer to three-dimensional growth of dots. The schematic graph of the process is shown in Figure 1.2(a). [3]
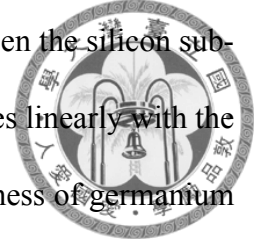
The strain relaxation in S-K mode can also occur from local elastic deformation of near surface layers. The schematic graph is shown in Figure 1.2(b) and this mechanism can only produce significant relaxation of an isolated island. [6]

1.3   Applications of Ge/Si Quantum Dots

Due to quantum confinement, the absorption and emission wavelengths can be tuned by simply varying the size of the quantum dots. As in Figure 1.3, the dot peak energy
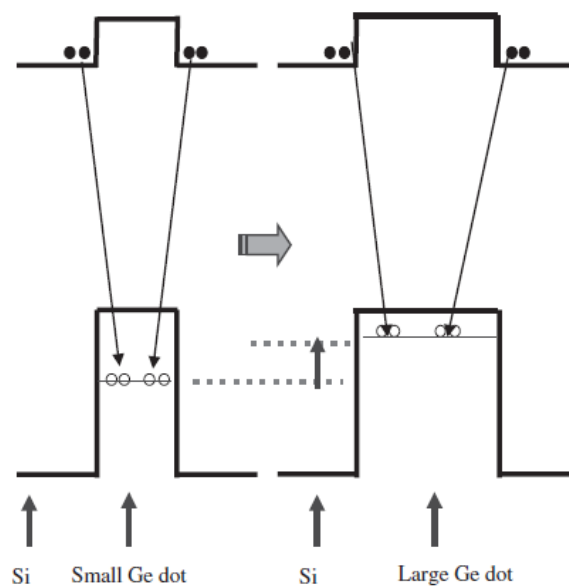
Figure 1.3: Schematic of quantum mechanical effect in germanium quantum dots

shifts with different dot sizes [7]. This makes quantum dots much more valuable in many applications such as quantum dots photodiodes, quantum dots LEDs, quantum dots lasers; and etc [8].
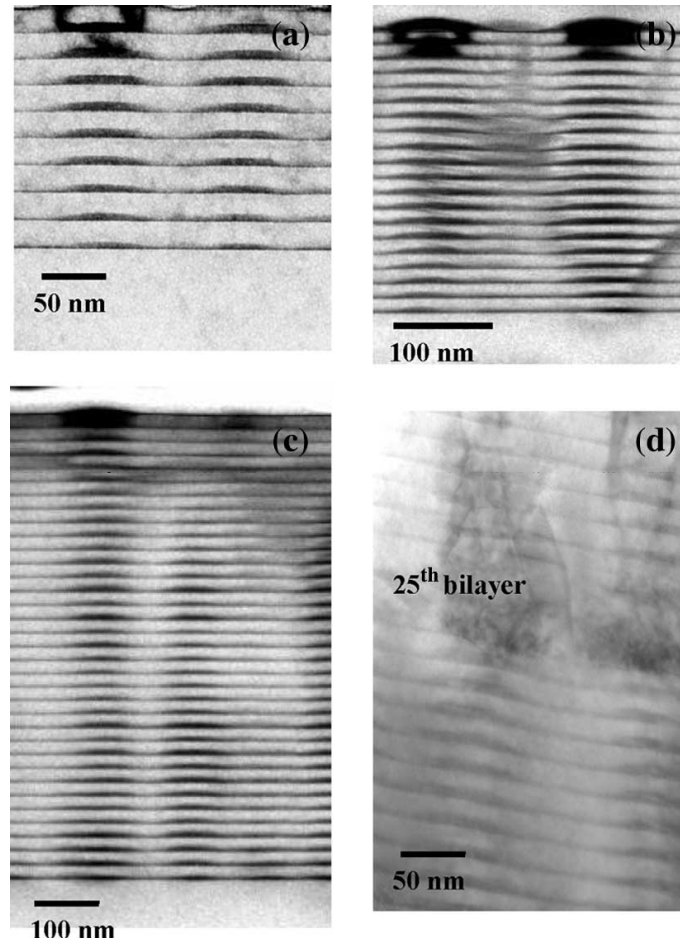
Figure 1.4: Cross-sectional TEM images of (a) 10, (b) 20, (c) 35, and (d) 50-period Si(20 nm)/Ge(1.5 nm) superlattice samples grown at 540 °C.

For Ge/Si quantum dots, it's more compatible than other materials to integrate optical and electronic devices on a silicon substrate by using well silicon VLSI technology to achieve low cost [9]. What's more, both silicon and germanium are non-poisonous compared to other materials such as GaAs or InAs. The growth of multilayered germanium-dot superlattices is also very important for applications of optoelectronics (Figure 1.4). It has turned out to be one of the most effective way to control the vertical and lateral arrangement of the dots [10]. Here we give a brief introduction over some of them.

1.3.1 Quantum Dot Photodiodes

Figure 1.5 (a) and (b) shows the schematic sketch of the photodioes with germanium quantum dots and its energy diagrams under zero bias. In the application of photodiodes, there are four advantages: (i) the optical transition polarized in the photodiode plane become allowed. This makes it possible to operate at a normal incidence of light without additional gratings or reflectors; (ii) oscillator strength is high from the localization of the carrier wave function along all three spatial coordinates; (iii) the lifetime of photoexcited carriers is long ($> 10^{-11}$ s) due to the high photoelectric gain from the low capture rate of carriers in a quantum dot; (iv) the dark currents are small in quantum dots photodiodes
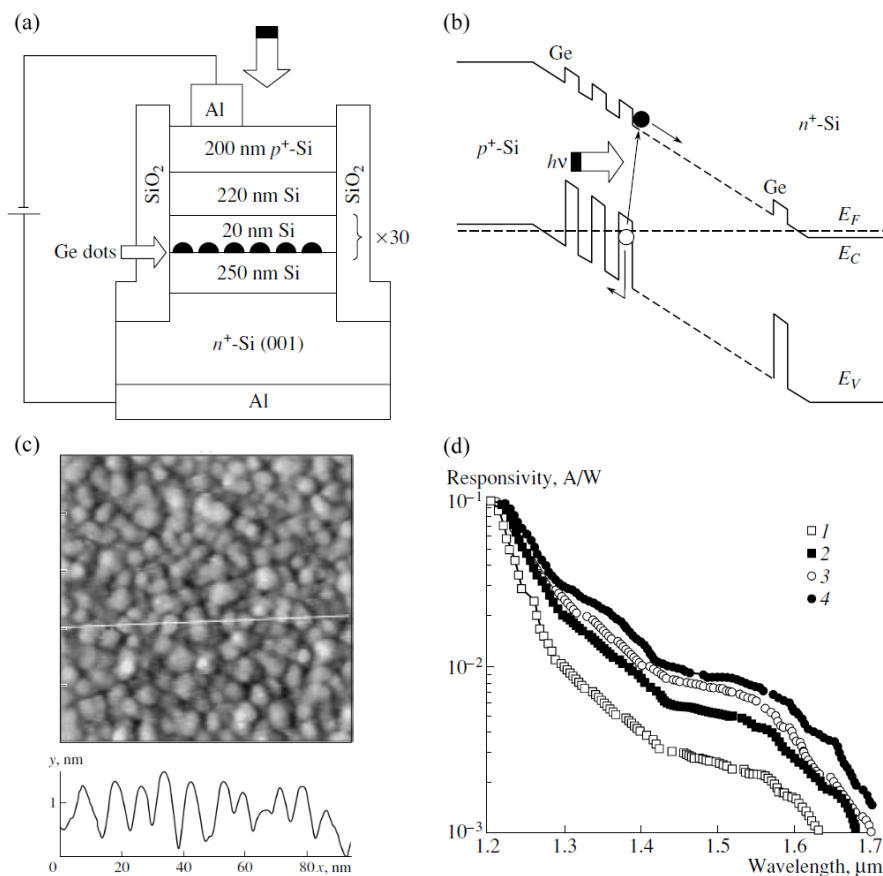
Figure 1.5: (a) Sketch of the cross-section of a p-i-n photodiode with germanium quantum dots. (b) The energy diagram fothe diode with zero bias. (c) SEM image of the quantum dots in size of 100×100 nm^2. (d) Current responsivity spectra at bias on (1)0, (2)0.2, (3)0.5, and (4)2 V.

because the energy spacings between the quantum dots levels are large with dot size less than 10 nm. The excited states of quantum dots is not involved in the processes of thermal generation of carriers in allowed bands.

The SEM scan of MBE-grown germanium quantum dots with lateral size about 8 nm and sheet density of about 1.2×10^{12} cm^{-2} is shown in 1.5(c). And the current responsivity recorded in room temperature is shown in 1.5(d). The lowest dark current density of about 2×10^{-5} A/cm^2 under 1 V reverse bias at room temperature was achieved, which shows the potentials of photodiodes with germanium quantum dots. Here, high sheets density of germanium quantum dots to increase the quantum efficiency and narrow dot size distribution to control the absorption spectrum are two main goals to reach. [11]

1.3.2 Quantum Dot LEDs

Due to the indirect band structure of silicon, the luminescence efficiency of Si-based structures is very low. Some efforts to make efficient light emitters was done by growth of the multilayered germanium quantum-dots superlattices. The LED was made with a p-i-n structure consisting of 10-period intrinsic multilayered germanium quantum dots
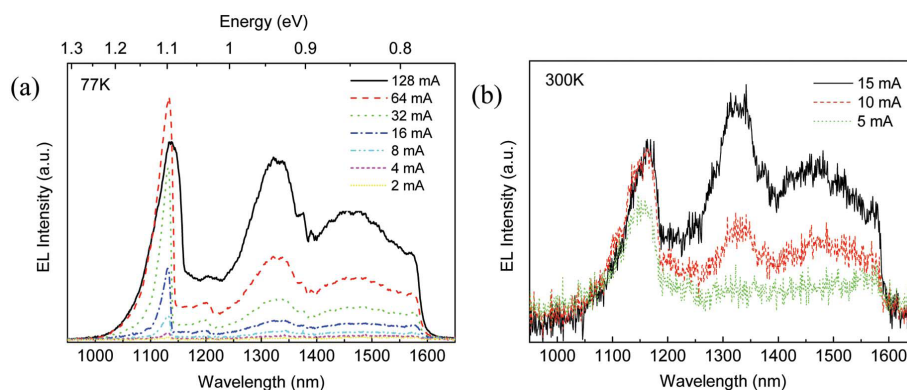
Figure 1.6: Electroluminescence spectra at different biases measured at: (a) 77 K and (b) 300 K

sadwitched with an n-type and a p-type silicon layers on an n-doped silicon (100) substrate. The electroluminescence spectra is shown in Figure 1.6. It shows that it can be operated in the near infrared spectral range around the 1.3-1.55 μm. However, the quantum efficiency is still low for practical application and remains a big challenge [9].
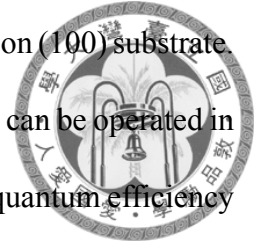
1.3.3   Quantum Dot Solar Cells
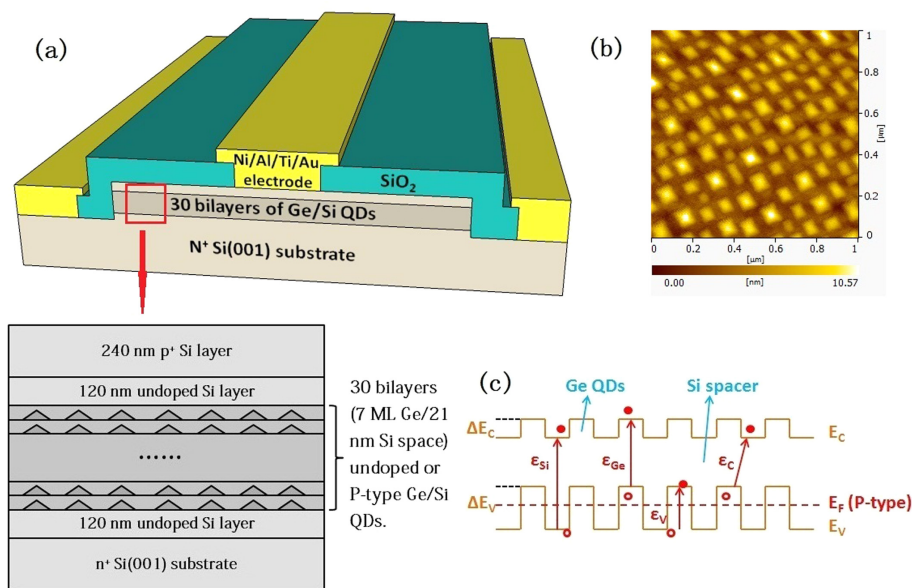
Figure   1.7:   (a) Cross-sectional view of Solar cells with germanium quantum dots. (b) AFM image of the grown Ge/Si quantum dots. (c) Band edge diagrams of multilayer.

In the field of solar cells, the increased external quantum efficiency in infrared region and the short-circuit densities make germanium quantum dots suitable to be included in the solar cells. Figure 1.7 (a) shows the schematic structures of the p-i-n solar cells with 30 bilayers undoped or p-type self-assembled Ge/Si quantum dots fabricated on n^+-Si(100) substrates by ultrahigh vaccum chemical vapor deposition. The AFM image of the grown quantum dots with sheets density about 2×10^{10} cm^{-2} is shown in Figure 1.7 (b). Figure 1.7 (c) is the four common types of band transitions in the Ge/Si quantum dots multilayer. ε_{Ge}, ε_C, and ε_V are dependent on germanium content and size of the germanium

dots. [12] Thus, it's also important in controlling the distribution of the size of the dots in the solar cells.

1.4 Control of the Growth of Ge/Si Quantum Dots

For many potential applications of optoelectronic, not only high sheet density of germanium quantum dots but the narrow size distribution are essential issues. Also, the spatial ordered of the quantum dots is essential for electronic applications. However, in most cases, dots grown in S-K mode exhibit poor lateral ordering because the dots nucleation is statistical in nature.

Therefore, some efforts were done to control the growth of germanium quantum dots and are introduced here.

1.4.1 Growth Through Nanostencil
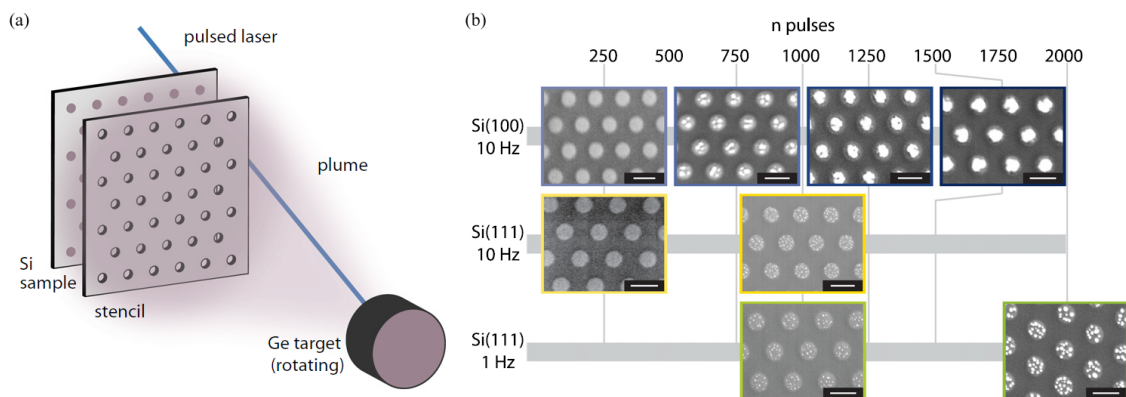
Figure 1.8: (a) Schematic graph of the sample geometry, showing the germanium target, the stencil, and the silicon substrate. (b) SEM images of patterned Ge structures formed at 600 °C via PLD through a nanostencil.

In this work, the germanium was grown by pulsed laser deposition (PLD) at 600 °C via nanostenciling. As shown in Figure 1.8 (a), the stencil with hexagonal arrays of circular apertures in 350 nm opened in freestanding was put on the silicon substrate and

Figure 1.8 (b) shows the results of growth. Below the critical thickness, smooth two-dimensional mounds are formed both on silicon(100) and (111). After thickness exceeds the critical value, the formation of three-dimensional dots begins. The dots on silicon(100) and (111) are quite different. The silicon(100) hosts a larger dots than silicon(111). On silicon(111), the dots remain discrete to at least 2000 laser pulses. The positioning of germanium quantum dots with average size of 274 nm in standard deviation of 25 nm was done [13].

1.4.2 Pre-Patterning

Growth of quantum dots on patterned substrate is also a way to control the position of the quantum dot formation not only for germanium on silicon but also for other quantum-dot materials. There are many ways of pre-patterning the substrate such as electron beam lithography [14], focused ion beam [15], nanoindentation [16], and etc. Figure 1.9 shows one of these works. The silicon(001) substrate was patterned by focused ion beam. And 8 monolayers of germanium is deposited on it by solid-source molecular beam epitaxy. At low temperature of 550°C, the kinetic is limited and the smaller islands are formed. The perfect ordered distribution of dots in the pits is observed. When the temperature is as high as 700°C. The kinetic of dots are quite larger. Thus they are not confined to form in

(a)   (b)   (c)
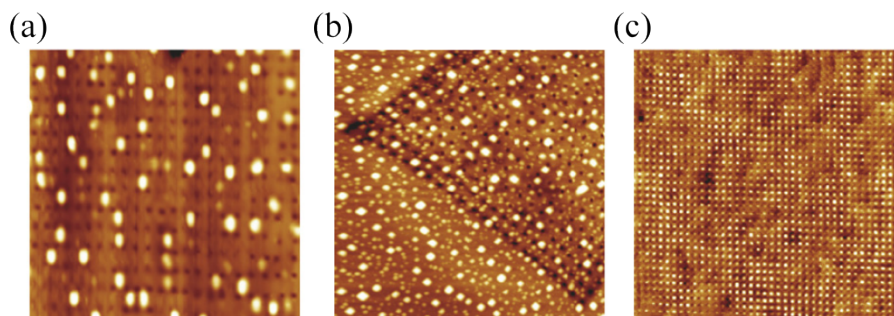
Figure 1.9: AFM images of the patterns after deposition of 7 monolayers of germanium at (a) 700°C, (b) 650°C, and (c) 550°C. All the images are in size of 2.5×2.5 μm^2.

the pits. At the intermediate temperature of 650°C, random distribution of dots both in the pits and outside the pits can be observed. The dots at 650°C are in the transition state from 550°C to 700°C. The pre-patterning is a good way to control the position of the dots. [17].
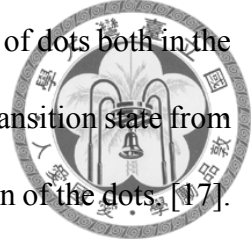
1.4.3 Laser Induced Periodic Surface Structure on Silicon

The irradiation of several materials with lasers is an interesting topic in many works. In this research, the laser-induced silicon nanodot array was observed by the irradiation on silicon surface with laser of wavelength 532 nm. The growth process of the laser induced periodic surface structure (LIPSS) is shown in Figure 1.10 (a). With fluence of 124 mJ/ cm^2 and repetition rate of 2 Hz, clusters of small dots first form randomly on the surface in stage I (initial stage). Then in stage II (intermediate stage), periodic ripple consisting of bands of smaller dots of 10 nm or less is formed. Finally in stage III (aligning stage), dots aggregate to become larger. The schematic process is shown in Figure 1.10 (b).
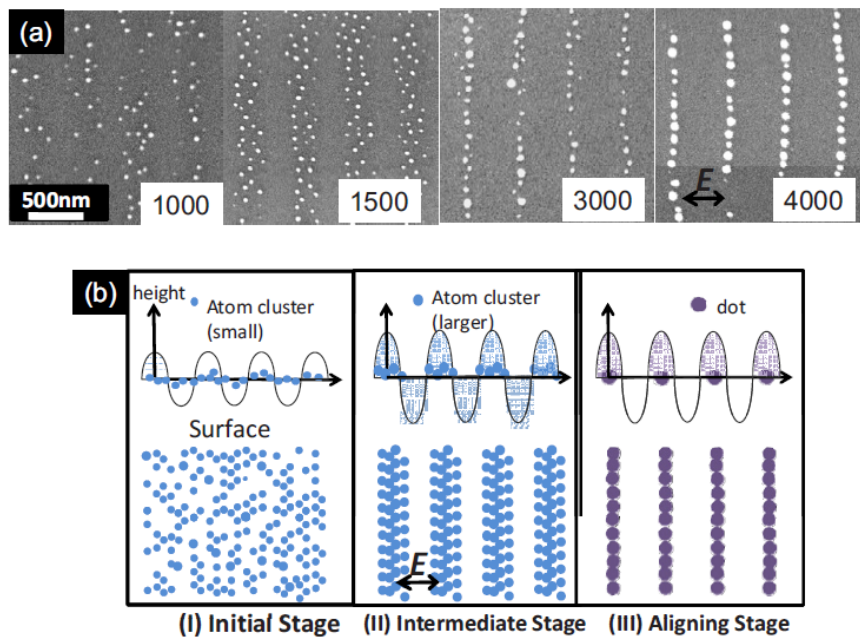
Figure 1.10: (a) SEM images of LIPSS-dots on silicon(100) surface after 1000, 1500, 3000, and 4000 laser shots. (b) Schematic graph of the formation process in three stage.

The AFM image and the line profiles of the LIPSS after 2000 laser shots is shown in Figure 1.11 (a) and (b). The dots within a ripple (horizontal direction) have subwavelength separation of approximately 120±10 nm, corresponding to a separation between 1/5 and 1/4 wavelength of the irradiated laser beam (532 nm). The period of the regular ripples of aligned dots (vertical direction) is about 530±25 nm, which is close to the wavelength of the incident laser. The results indicate that it might be due to not only a top-down process of the interference between the incident laser light and the scattered waves on the surface, which predominates the regular ripple formation at a laser wavelength, but also a bottom-up process involving the self-organization of the atomic clusters generated on a surface by a laser shot. [18]

1.4.4 Laser Irradiation on Germanium Quantum Dots

The research of irradiation on the grown germanium quantum dots with laser is introduced here. The germanium quantum dots were grown by solid-source molecular beam epitaxy (SS-MBE) at 500 °C. As shown in Figure 1.12, the size distribution of the deposited dots is separated into two parts: (i) domes with mean height of about 18 nm and
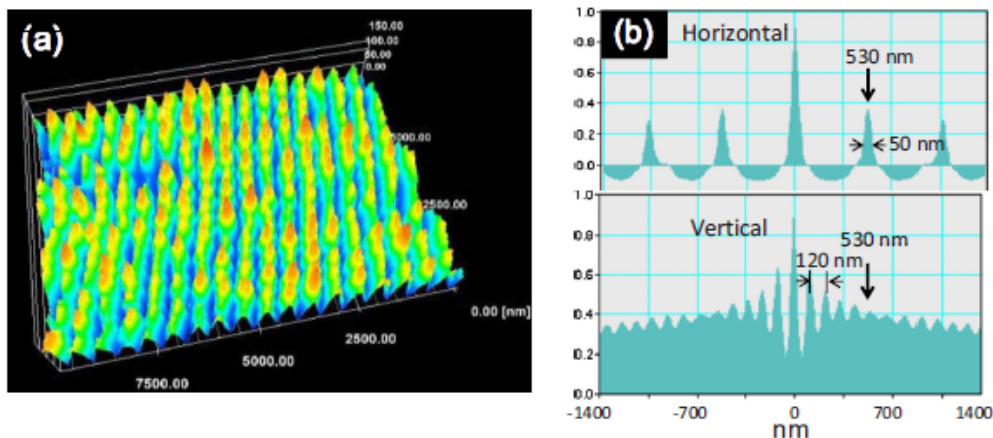
Figure 1.11: (a) AFM image of LIPSS-dots after 2000 laser shots. (b) Line profiles along horizontal and vertical direction.

mean base length of about 130 nm; (ii) pyramids with mean hight of about 5 nm and mean

base length of about 50 nm.
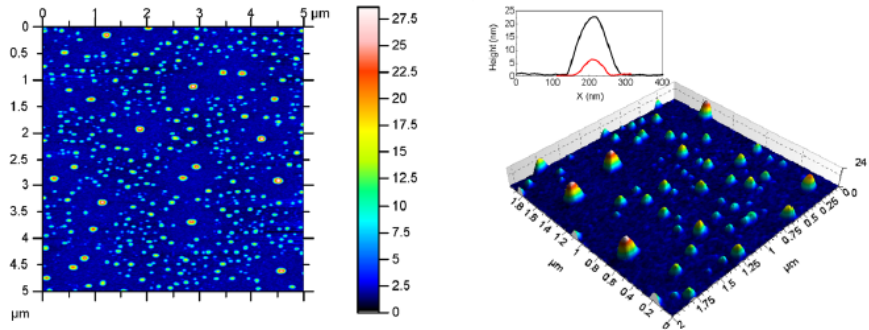
Figure 1.12: Top view and 3D view of the grown germanium quantum dots by SS-MBE at 500 °C. The line profiles is the profile of dome (black) and pyramid (red).
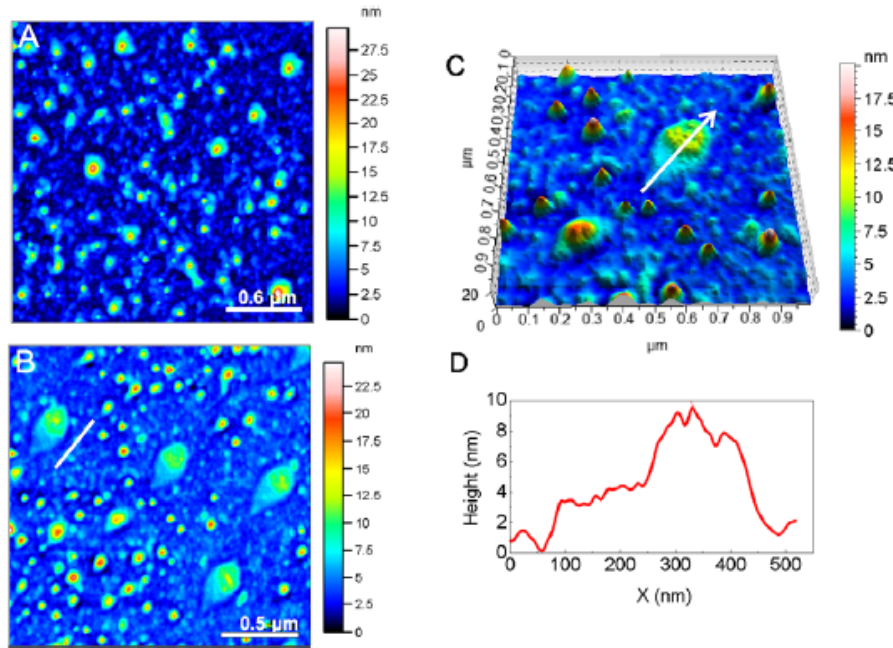
Figure 1.13: (a)(b) AFM images of the laser irradiated germanium quantum dots. (c) 3D view of the AFM image. (d) Line profile of a irradiated dome in (c).

After irradiation of 800 shots by the 10-Hz laser with wavelength of 532 nm, an evident change in the quantum dots is observed in the region with laser fluence of about 50 to 110 mJ/cm^2. In Figure 1.13 (a), the quantum dots appear bigger and more irregular in shape. In the same region with lower fluence, quantum dots show a remarkable morphology (Figure 1.13 (b) and (c)). Domes and the largest pyramids show and elon-

gated character along the (100) directrion independent of their location. [19] However, the positioning and size control of the quantum dots wasn't be reached in this research.

1.5   Motivation and Gaols

There are big potentials in the applications of Ge/Si quantum dots in optoelectronics. The energy bandgap can be tuned by the size of dots due to the quantum confinement, so the wavelength of absorption can be tuned for several applications. The silicon based devices make it cheaper and convenient for the silicon VLSI technology. Poisonous materials of silicon and germanium can reduce the environmental impact in the manufacturing processing.

However, due to the nature statistical size distribution from the S-K mode growth, there are some restrictions of the application from the broadening of the absorption spectra. Therefore, control of the growth of germanium quantum dots is quite important. We've seen the control of growth by pre-patterning and laser irradiation on the grown germanium quantum dots. In our research, we use pulsed laser deposition (PLD) to grow the germanium on silicon quantum dots, trying to find out the critical thickness of the formation of quantum dots. And we irradiate the laser on the grown germanium thin film on silicon substrate where the quantum dots are not yet formed. We hope to see some laser-induced quantum dots formation and figure out the dependence of the morphology of quantum dots on irradiated laser fluence, film thickness, and irradiated laser shot numbers.

Chapter 2

Materials and Methods

2.1 Pulsed Laser Deposition

2.1.1 Introduction to Pulsed Laser Deposition

Pulsed laser deposition (PLD) is a simple and common technique. It has been shown to be a versatile technique for growing thin films of a wide range of materials, from single atomic layer to quasi-bulk crystalline films. The fundamental setup of PLD is shown in
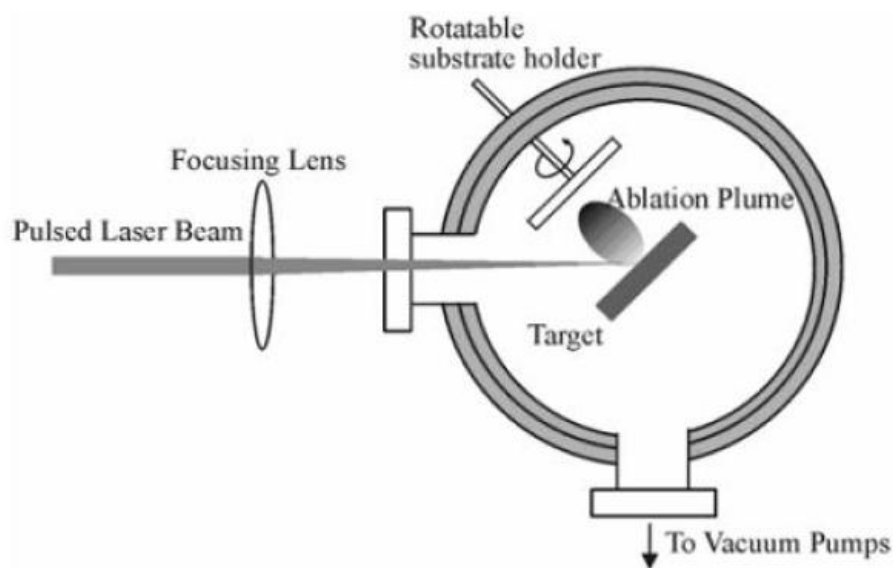
Figure 2.1: Basic setup of pulsed laser deposition.

Figure 2.1 [20]. The beam of a high power pulsed laser goes into the vacuum chamber,

focused on the target by lens. Due to the high fluence, the laser heat the surface of the target and then vaporize the target to form plasma plume, which consists of atoms, diatoms, molecular, and ions. The ablation plume then deposit on the substrate to form thin films.
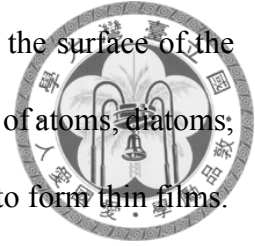
2.1.2 The Mechanism of Pulsed Laser Deposition

There are two mechanism of PLD depending on different pulse duration of the laser. In the process of nanosecond PLD, the pulse duration of laser is long enough to heat the target and form the plasma by ionization of the surface of the target. This process is called absorption process. In the process of femtosecond PLD, the duration is too short for heating the target. The electrons are ionized first and then collide the surface of the target to form plasma. The ionized electron is called seed electron and the process is called the nonabsorption process. The schematic graph of the process is shown below:
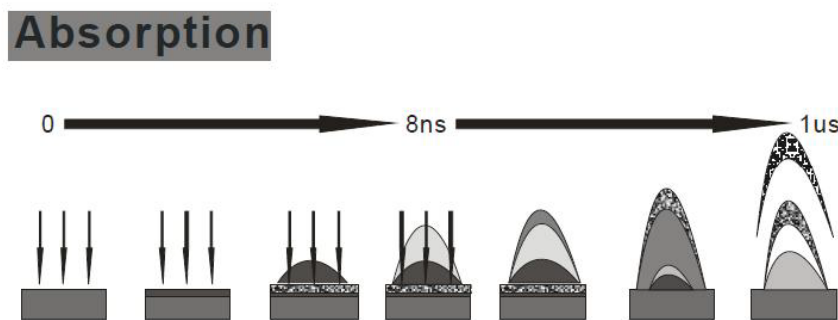
Figure 2.2: Absorption process in PLD.

Absorption process:

1. Initial absorption of laser radiation.

2. Melting of the target surface.

3. Vaporization and ionization.

4. Formation and thermal equilibrium of the plasma.

5. Forward propagation and division of the plasma after expansion.

6. Cooling and slowing down of the plasma.

7. Collapse of the plasma and deposition of the material.
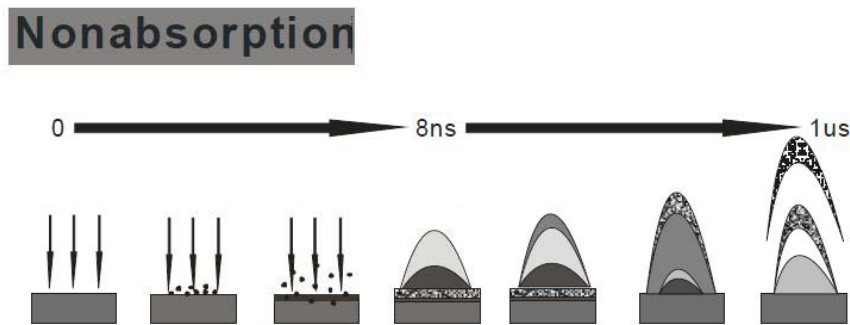
Figure 2.3: Nonabsorption process in PLD.

Nonabsorption process:

1. Formation of enough electromagnetic field for ionization by laser.

2. Ionization of seed electrons.

3. Heating of surface by the electron-phonon relaxation.

4. Formation of the plasma from ionization of the target surface by seed electrons.

5. Forward propagation and division of the plasma.

6. Cooling and slowing down of the plasma.

7. Collapse of the plasma and deposition of the material. [21]

2.1.3 Dependence of Laser Fluence

Figure 2.4 is the schematic graph of the dependence of the plasma propagation on the laser fluence. When the fluence of the laser is higher, more plasma will form from the absorption of the target, which increase the kinetic energy of the plasma and results in nucleation of smaller clusters. Therefore, larger fluence of laser results in larger deposition. [22] For the growth mechanism of S-K mode of the germanium quantum dots, please see Section 1.3.
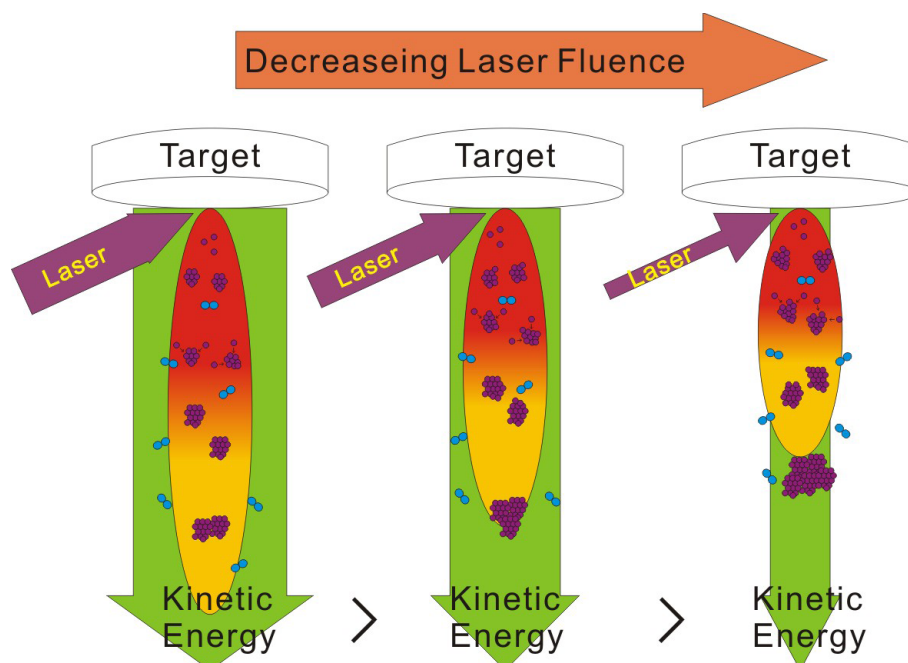
Figure 2.4: Dependence of plasma propagation on laser fluence.

2.2 Experimental Methods of Pulsed Laser Deposition

2.2.1 Light Source of Ablation Beam in PLD

As shown in Figure 2.5, the light source we use as the ablation beam in the system of pulsed laser deposition is the Pro-350 Nd:YAG pulsed laser manufacturing from Quanta-Ray. The wavelength of the laser is the third harmonic wavelength of 355 nm.

The specifications of Pro-350 is shown below:

- Wavelength: 355 nm.

- Maximum pulsed energy: 350 mJ.

- Pulse duration: 8 ns.

- Repetition Rate: 10 Hz.

- Beam size from the output: 12 mm in clear aperture.
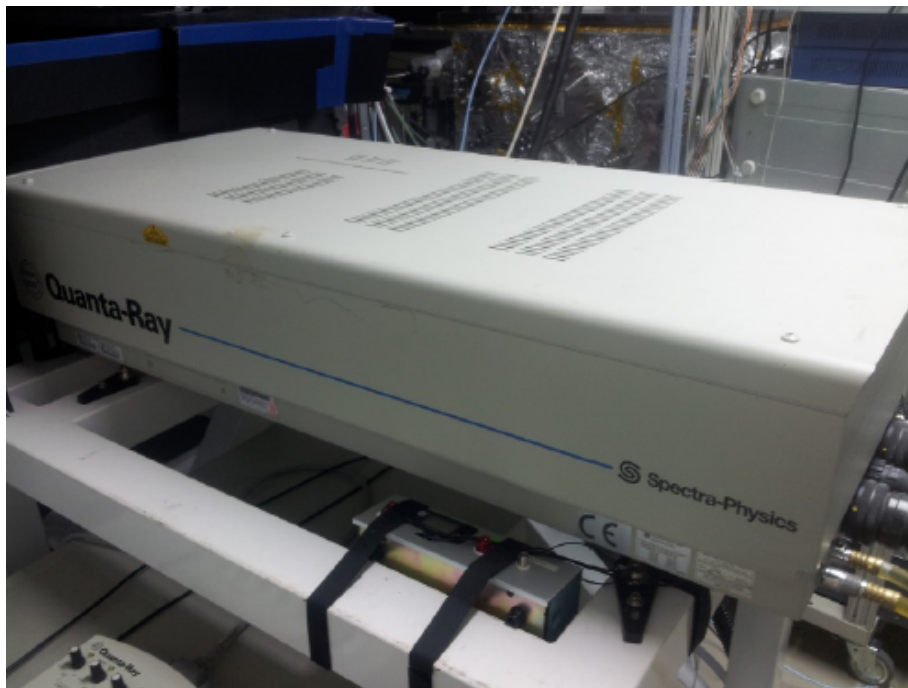
Figure 2.5: Light source of PLD: Quanta-Ray Pro-350 Nd:YAG pulsed laser.

2.2.2 Experimental Setup of PLD

Figure 2.6 shows the schematic setup of the pulsed laser deposition in our experiment. In the vacuum chamber, the ablation beam is focused by the lens and irradiates the target in direction of 45°. By tuning the position of the lens, the on-target beam size is tunable. The photo of the setup is shown in Figure 2.7.
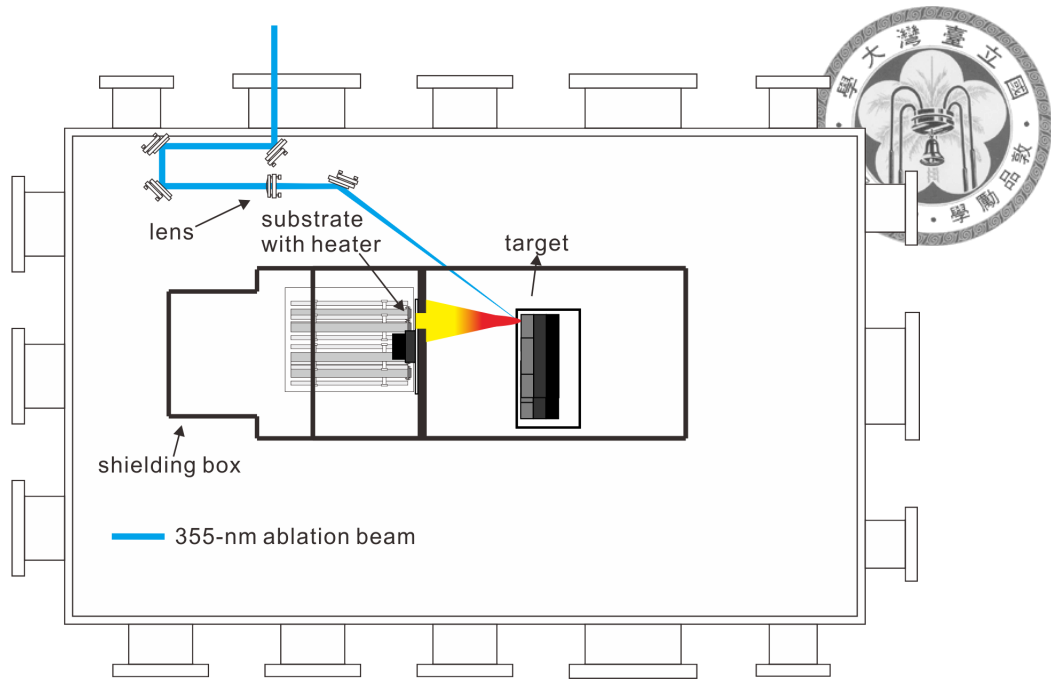
Figure 2.6: Schematic setup of pulsed laser deposition.
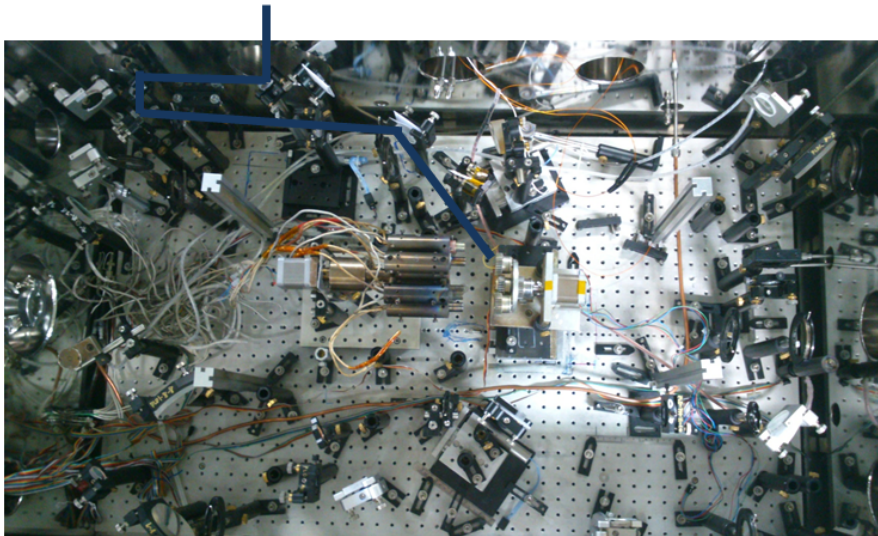
Figure 2.7: Photo of the setup of pulsed laser deposition.

Inside the PLD chamber, there are several instruments as follows:

• Target holder (Figure 2.8): It can hold five targets and keep rotating by the motor behind it while laser beam irradiated on the target. There is another motor to rotate the position of the targets to switch another one. Thus we can do PLD with several materials of targets in one run without breaking pressure.

- Substrate holder (Figure 2.9): It can hold six substrates and there are five of them consisting a heater system to heat and anneal the substrates. We can do PLD with six substrates in one run to save the time of vacuuming.
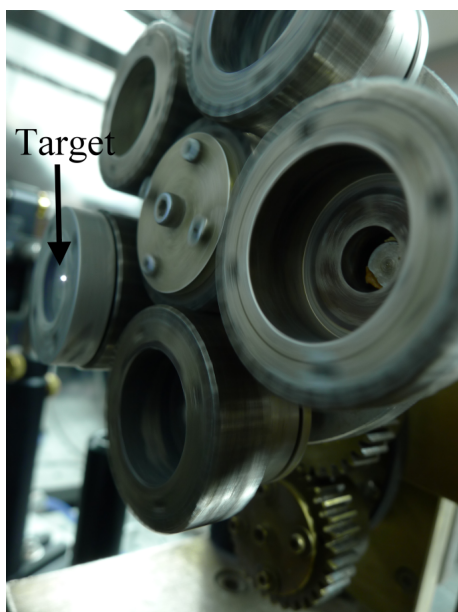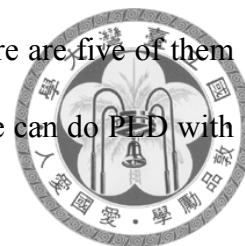
Figure 2.8: Rotating target holder.
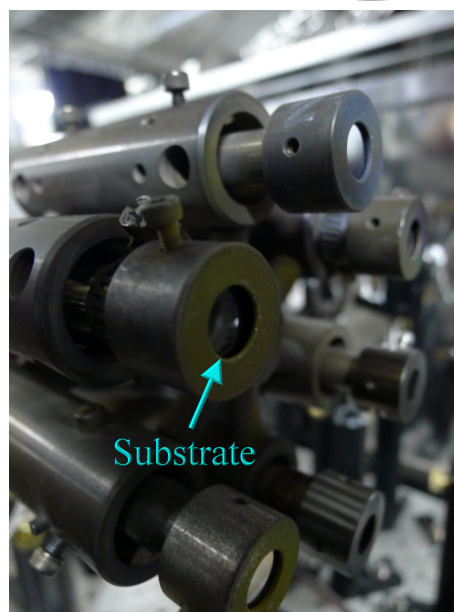
Figure 2.9: Substrate holder.

- Thickness monitor (Figure 2.10): The thickness monitor is of model SQM-160 from Sigma Instruments. On the sensor of thickness monitor (Figure 2.10 (a)), there is a quartz crystal oscillating during the growth of film. When the film grown on the crystal becomes thicker, the oscillation frequency of the crystal becomes lower. Thus the thickness and the deposition rate can be calculated and be shown on the controller (Figure 2.10 (b)). To make sure that the deposition rate is the same in every experiments, we use it to record the thickness. We also use it to find out the relation between deposition rate and several parameters.

(a) (b)
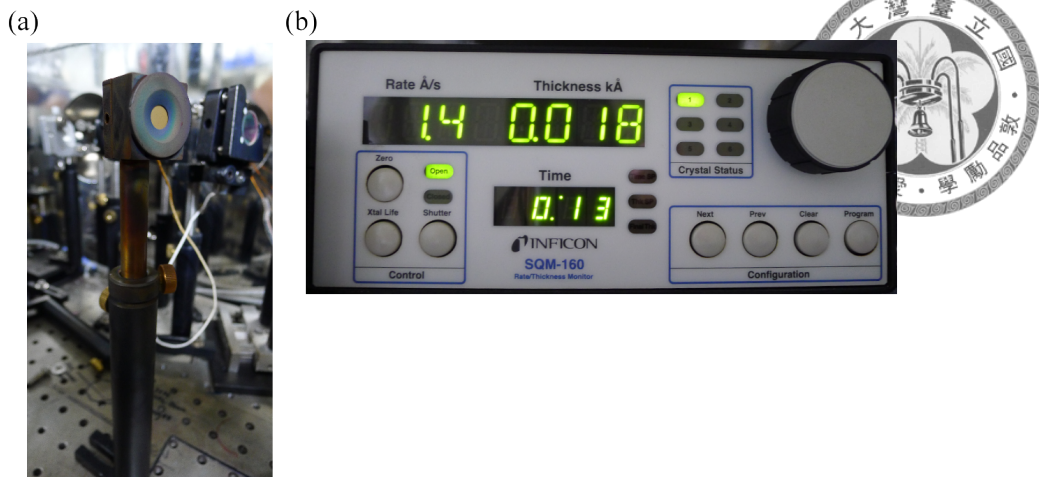
Figure 2.10: (a) Thickness monitor and (b) its controller.

2.2.3 Issue of the Air Pressure in PLD Chamber

The lowest air pressure in our chamber can be pumped to only 5.37×10^{-4} torr in 80 minutes, which might not be low enough to slow down oxidation of the silicon substrate after cleaning. Therefore, a cold trap of about -170 °C, with flowing liquid-nitrogen-cooled air inside, is introduced to adsorb H_2O and CO_2 in air and thus can lower the pressure. As shown in Figure 2.11, with a cold trap, the pressure can achieve 1.37×10^{-5} torr in 20 minutes. Although the pressure might still not be low enough, the reducing of H_2O in air, witch participates a lot in the process of oxidation could also slow down the oxidation of the silicon substrate.
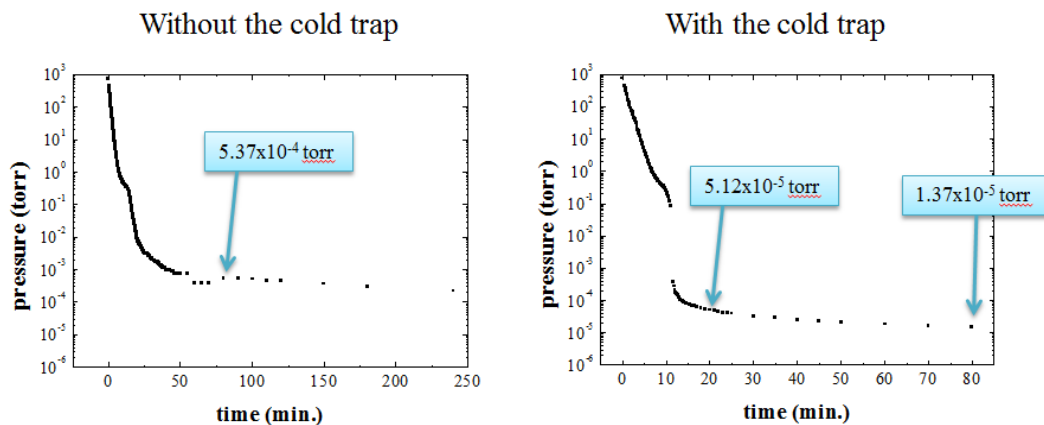
Figure 2.11: Pressure of the chamber versus vacuuming time with and without cold trap.

2.2.4 Details of the Target and Substrate

The details of the target and the substrate are shown below:

Target

- Material: Germanium (Ge).

- Diameter: 20 mm.

- Thickness: 5 mm.

- Purity: 99.9999%.

Substrate

- Material: Silicon (Si).

- Orientation: <100>.

- Type/Doping: P type/ Boron doped.

- Thickness: 275 ± 25 μm.

- Resistivity: $1\sim20$ Ω-cm.

2.2.5 Preparation of the silicon substrates

The silicon wafer with diameter of 4 inch was cut into pieces of 1×1 cm^2 by laser on the back side and grid lines of 2×2 cm^2 is curved by the laser on the front side(Figure 2.12). The grid lines are mark of the position so we can recognize different position irradiated control beam in many diagnoses of the samples.
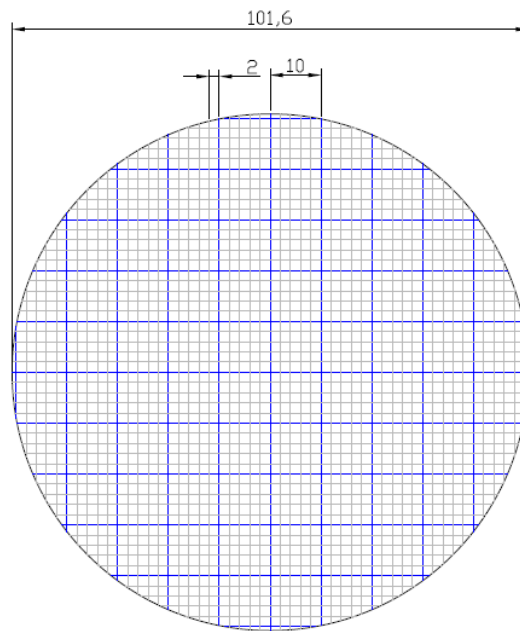
Figure 2.12: The cutting lines (Blue lines) of silicon wafer on the back side and grid lines (gray lines) on the front side. All the numbers are in unit of mm.

Before being growth, the silicon substrate was cleaned by the following procedures to remove the oxidation and contamination:

1. Dip the substrate in the teflon beaker with DI water:HF=1:50 for 4 mins.

2. Dip the substrate in the teflon beaker with DI water:HF=1:100 for 5 mins.
   (To remove the oxidation on the surface of the substrate.)

3. Flush the substrate with DI water.
   (To remove small particles on the surface of the substrate.)

4. Rinse the substrate in IPA(Isopropyl alcohol)
   (To remove the water marks on the surface of the substrate.)

5. Dry the substrate with nitrogen gas.

2.2.6 Determination of the Fluence of Ablation Beam

To determine the fluence of ablation beam, we first find out the relation between deposition rate and fluence. This was done by putting the thickness monitor 4 cm away from the target in the normal direction. The results is shown in Figure 2.13 (a). We found out that the deposition rate at fluence between 150 to 200 J/cm^2 is stable, with average absolute deviation of about 7%. In the range of stable fluece, the deposition rate won't change a lot from the fluctuation of laser fluence. Thus we picked 160 J/cm^2, which is in the range of the stable fluence, as our ablation beam fluence. With this fluence, we grew a very thick germanium film on silicon for 60 minutes and scan the sample with surface profiler which will be mentioned in Section 2.4.1. Figure 2.13 (b) is the results of surface profiler. The thickness of the film is about 208 nm. Therefore, we get the calibration value of deposition rate of about 3.467 nm/min. from the thickness of the film we grew.
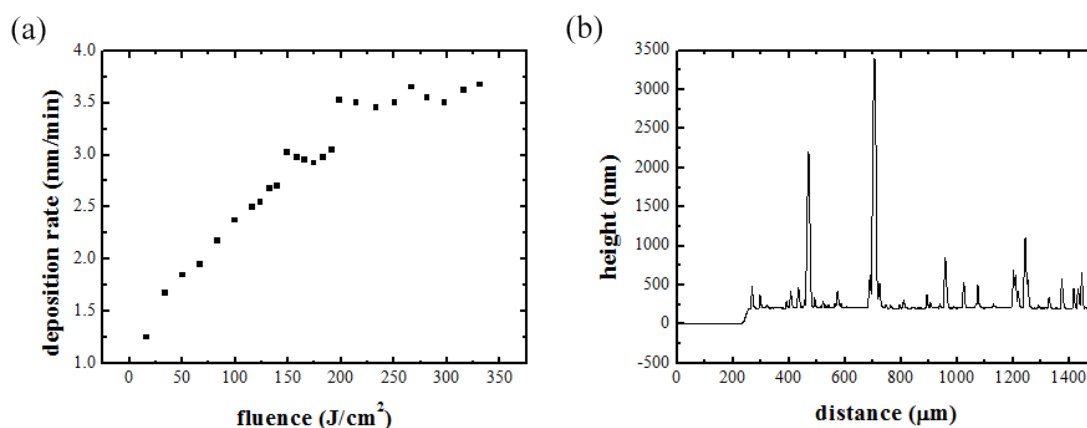
Figure 2.13: (a) Fluence versus deposition rate measured by thickness monitor. (b) Thickness measured by surface profiler after growth time of 60 minutes at fluence of 160 J/cm^2.

2.3   Experimental Methods of Control Beam

2.3.1   Light Source of Control Beam

In our experiment, we introduce another laser beam shown in Figure 2.14 to irradiate on the grown germanium thin film. The laser is Surelight manufacturing from Continuum. It's also a Nd:YAG pulsed laser with third harmonic wavelength of 355 nm. The specification is shown below:

- Wavelength: 355 nm.

- Maximum pulse energy: 100 mJ.

- Pulse duration: 8 ns.

- Repetition Rate: 10 Hz.

- Beam size from the output: 10 mm in clear aperture.
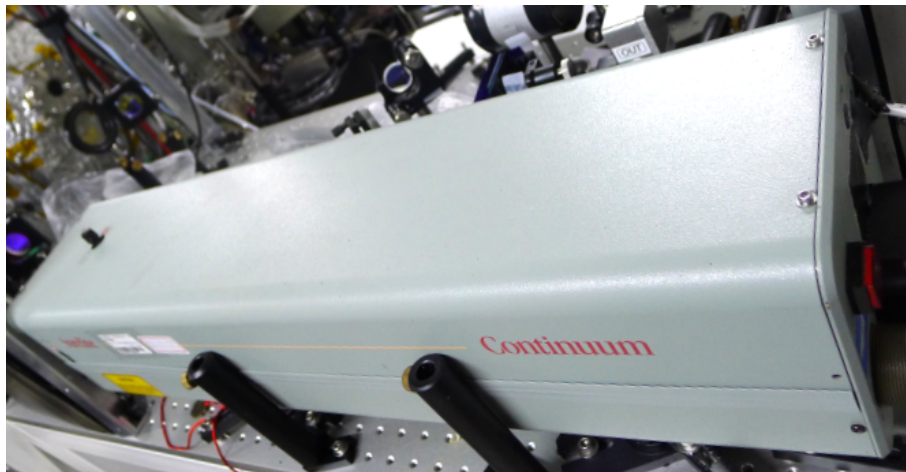
Figure 2.14: Light source of control beam: Continuum Surelite Nd:YAG pulsed laser.

2.3.2 Experimental Setup of Control Beam

The schematic setup of the control beam is shown in Figure 2.15. The beam goes

straight inside the chamber and is aligned to irradiate the substrate in normal direction.
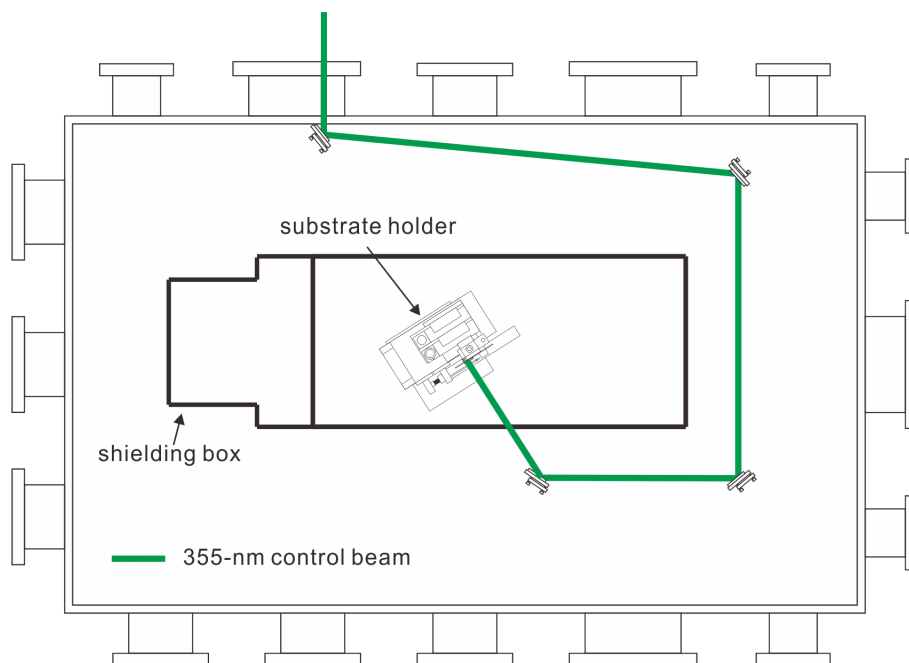
Figure 2.15: Schematic setup of control beam.
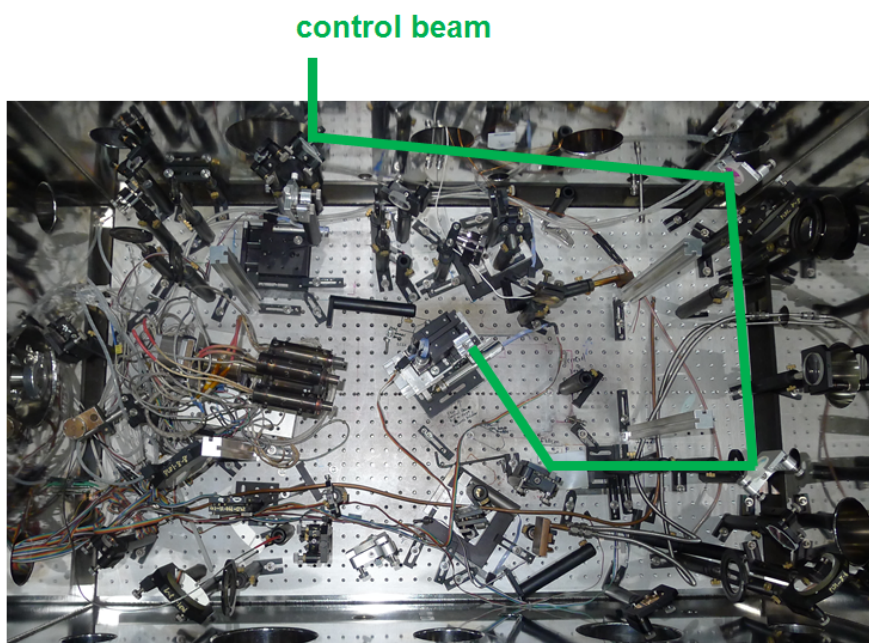
Figure 2.16: Photo of setup of control beam.

On the position of substrates, a substrate holder with two motorized linear translation stages in different direction is used (Figure 2.17). The holder allows us to put eight samples inside the chamber to be irradiated by the control beam in one run. We could switch from one target to the other precisely by the precision stages. The cold trap shown in 2.2.3 is introduced again to lower the air pressure.
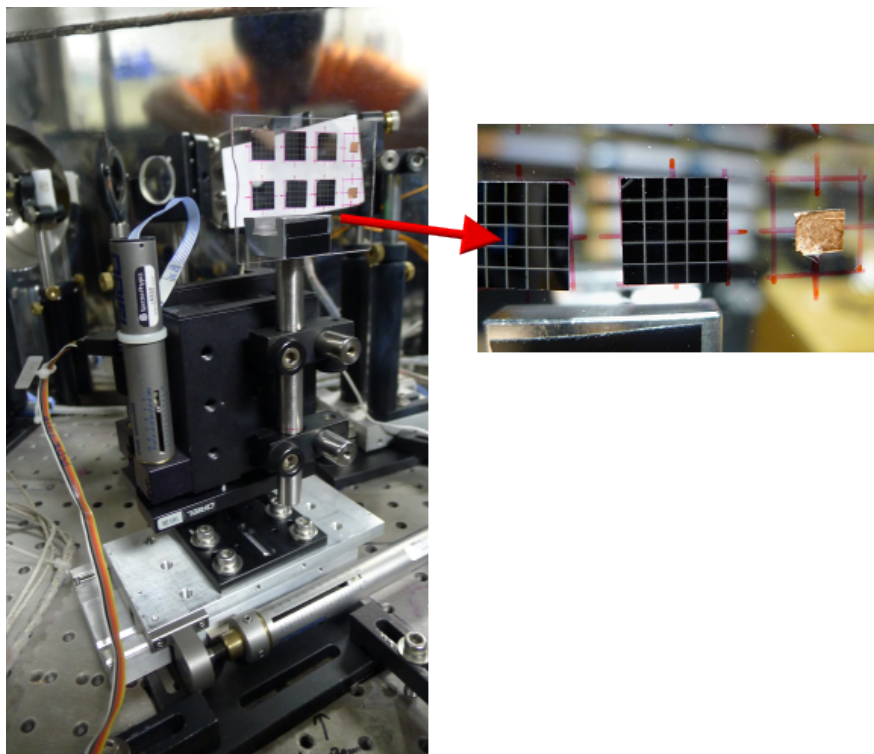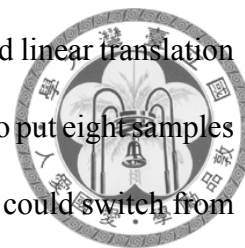
Figure 2.17: Photo of substrate holder.

2.3.3 Determination of Wavelength and Fluence of Control Beam

As shown in Figure 2.18 [23], among the original wavelength of 1064 nm, the second harmonic wavelength of 532 nm, and the third harmonic wavelength of 355 nm from the Nd:YAG laser, the absorption of the germanium at wavelength of 355 nm is the largest. We thus choose the third harmonic wavelength of 355 nm as our wavelength of control beam.

In order to make the grown germanium film irradiated by control beam and not be

ablated. We put the thickness monitor in front of a germanium wafer which is irradiated by control beam and we measure the thickness of the deposited germanium film from the ablation of the germanium wafer. If the wafer is ablated, we can know from the thickness monitor. The results is shown in Figure 2.19. Therefore, we choose the fluence of control beam below 80 mJ/cm^2.
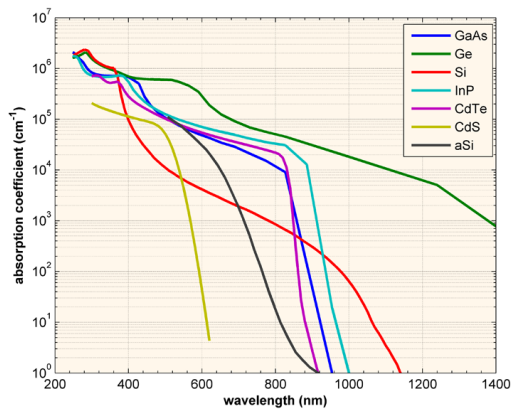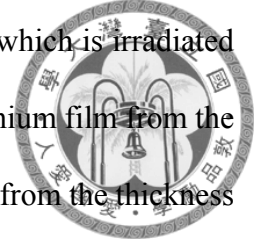
Figure 2.18: Absorption coefficient versus wavelength for several materials.
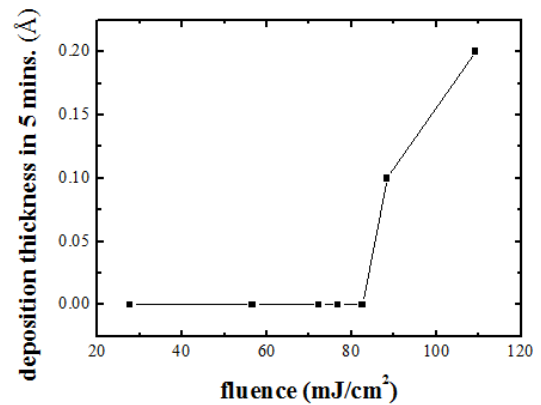
Figure 2.19: Ablation of the germanium wafer by control beam with different fluence. This is measured form the thickness of deposited film from the ablation of the germanium wafer in 5 minutes by the thickness monitor.

2.4 Diagnostic Tools

We introduce several diagnostic tools to get the information of the grown samples.

2.4.1 Surface Profiler

With a stylus tip in contact with sample and moving laterally across the sample for a specified distance and specified contact force, one can measure the variations of height on the scan line of the surface. Here we use it to measure the film thickness as shown in Section 2.2.6.
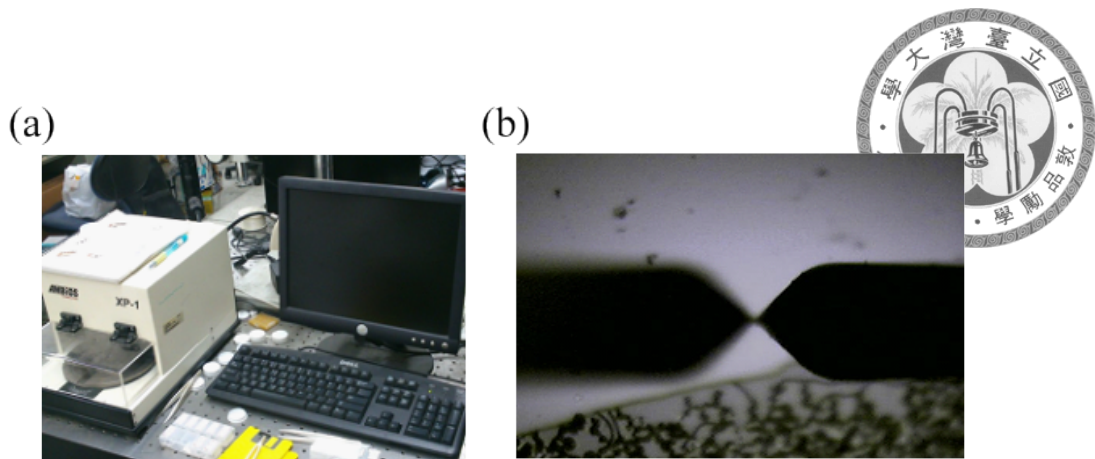
Figure 2.20: (a) Photo of the surface profiler we used and (b) its stylus tip.

The surface profiler we used is model XP-1 made from Ambios Technology (Figure 2.4.1). The specification is shown below:

- Vertical resolution: 1.5 Å at 10 μm, and 15 Å at 400 μm.

- Stylus tip radius : 2.5 μm.

- Maximum scan length range : 25 mm.

2.4.2 Atomic Force Microscopy

By the sharp tip (probe) at the end of the cantilever, the atomic force microscopy (AFM) provides us a good way to measure the two-dimensional morphology in the scale from nanometers to micrometers. The basic principle of the AFM is shown in Figure 2.21 (c) [24]. By Hooke's law, the cantilever bends due to the force between the tip and the surface of the sample. The bending can be recorded by using the laser beam reflected from the top surface of the cantilever into the photodiode array. The relative height of the surface can be calculated by the position of the laser irradiated photodiode array.
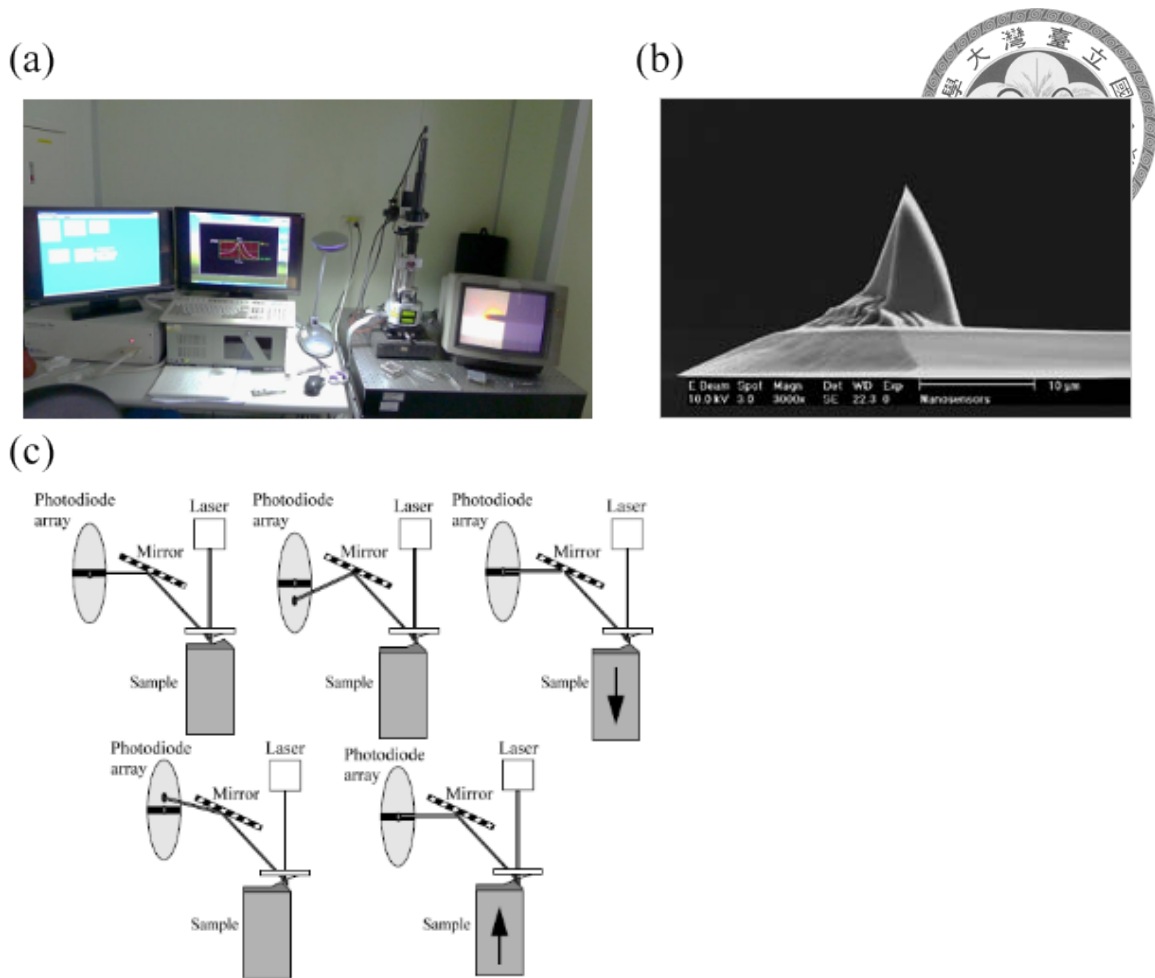
Figure 2.21: (a) Photo of the AFM we used. (b) The tip we used. The scale bar is in 10 μm. (c) Schematic of basic principles of AFM.

Figure 2.21 (a) and (b) [25] are the AFM and the tip we used, respectively. The AFM is MultiMode SPM made from Digital Instruments. And the tip is PointProbe Plus form Nanosensors. The specifications are shown below:

- AFM mode: Tapping mode.

- AFM tip radius of curvature < 10 nm

- Largest field of view: 15×15 μm.

2.4.3 Field Emission Scanning Electronic Microscope

With a focused electron gun emitting on the sample and the detector of secondary electron from the surface of the sample emitted by the electron beam, the scanning electronic microscope (SEM) allows us to see images in the nanometer scale. The basic scheme of the SEM is shown in Figure 2.22 (a) [26]. The ability of field emission scanning electron microscope (FE-SEM) to produce smaller focused electron beam provides us excellent images with spatial resolution down to 1 to 2 nm, which is 3 to 6 times better than conventional SEM.

(a)   (c)
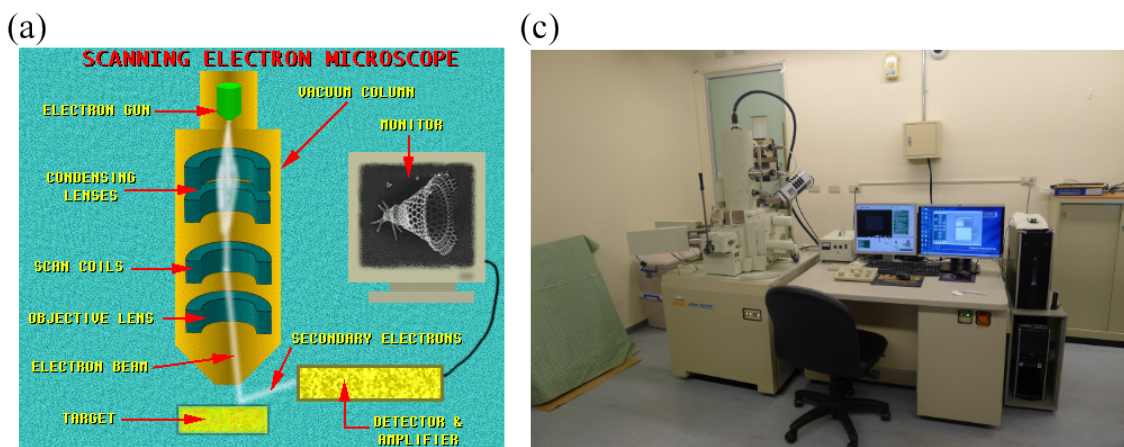
Figure 2.22: (a) Basic scheme of SEM. (b) The photo of FE-SEM we used.

Figure 2.22 (b) shows the FE-SEM we used, which is of model JSM-7600F from JEOL. The specifications are shown below:

- Resolution: 1.0 nm (15kV), 1.5nm (1kV).

- Magnification: $\times 25 \sim 10000000$.

- Accelerating voltage: $0.1 \sim 30$ kV.

- Electron gun: Schottky Electron Gun.

31

2.5   Experimental Procedures

In our experiments, we first grew germanium films on silicon (100) with different substrate temperatures to find out the temperature to grow. And grew films of different thickness, finding out the critical thickness for the spontaneous S-K mode self-assembled quantum dots by scanning the samples with AFM. Further check was done on one sample by scanning of FE-SEM.

Then we grew germanium films of thickness lower than the critical thickness and irradiated the control beam on the grown samples with different fluence and check the change of morphology by AFM.

The results will be shown and discussed in the next chapter.

Chapter 3

Experimental Results and Discussion

3.1 Growth of Germanium Quantum Dots

In our experiments, we first grew germanium on silicon substrate by pulsed laser deposition with various substrate temperature and various film thickness. The fixed parameters of the experiments is shown below:

- On-target beam size of ablation beam: 375 µm in clear aperture.

- Incident angle of ablation beam to target: 45°.

- On-target peak fluence of ablation beam: 160 J/cm^2.

- Distance from the target to the substrate: 4 cm.

- Air pressure during deposition $\sim 10^{-5}$ to 10^{-4} torr.

3.1.1 Films of Various Substrate Temperature

The results in AFM scan of germanium films with various substrate temperatures and the same effective thickness of 43 Å (30.7 ML) is shown in Figure 3.1. Here, one

monolayer (ML) of germanium equals to thickness of 1.4 Å [27]. It shows that at this thickness only with the substrate temperature of 400 °C can the formed quantum dots be the smallest among them. Thus we choose 400 °C as our substrate temperature.

(a) **(b)** **(c)**
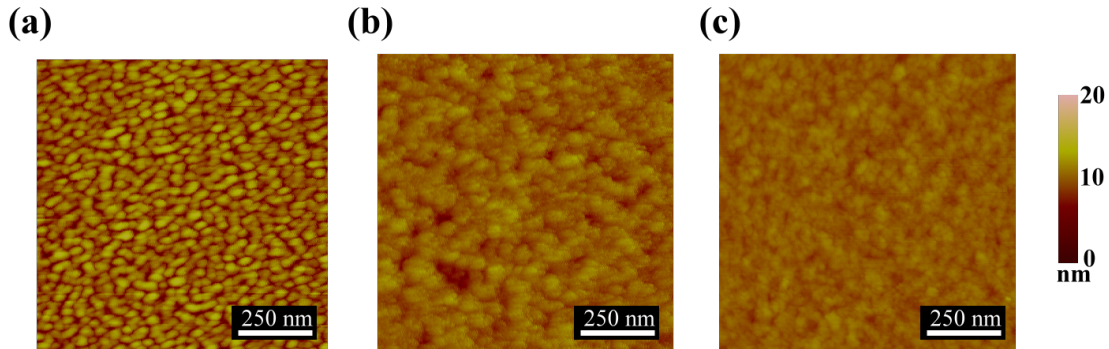
Figure 3.1: AFM scans of germanium films with substrate temperatures of (a) 400 °C, (b) 500 °C, and (c) 600 °C.

3.1.2 Films of Various Effective Thickness

At growth temerature of 400 °C, the results in AFM scan of germanium films with various effective thickness are shown in Figure 3.2. In the scan of the effective thickness of 14 Å (10.0 ML), the film is flat without any dots formation. Some dots formed with the effective thickness of 18 Å (12.9 ML). The dots might be formed from the local deformation of the film with the mechanism shown in Section 1.3. The 3D view and line

(a) **(b)** **(c)**
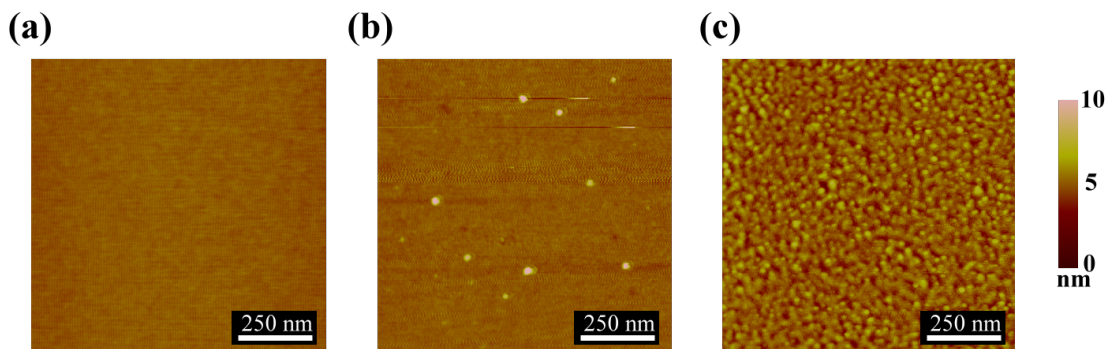
Figure 3.2: AFM scans of germanium films with effective thickness of (a) 14 Å (10.0 ML), (b) 18 Å (12.9 ML), and (c) 22 Å (15.7 ML).

profile of one dot is shown in Figure 3.3 (a). The height of the dot is about 7 nm and the base diameter is about 36 nm. When the effective thickness of films is 22 Å (15.7 ML), we saw high density of dots, with height of about 2 nm and base diameter of about 32 nm (Figure 3.3 (b)). Further scan of SEM with film thickness of 22 Å (15.7 ML) in Figure 3.3 (c) was done to double-check. Therefore, in order to irradiate the control beam on the film without quantum dots, we choose the thickness less than 14 Å (10.0 ML) or 18 Å (12.9 ML).
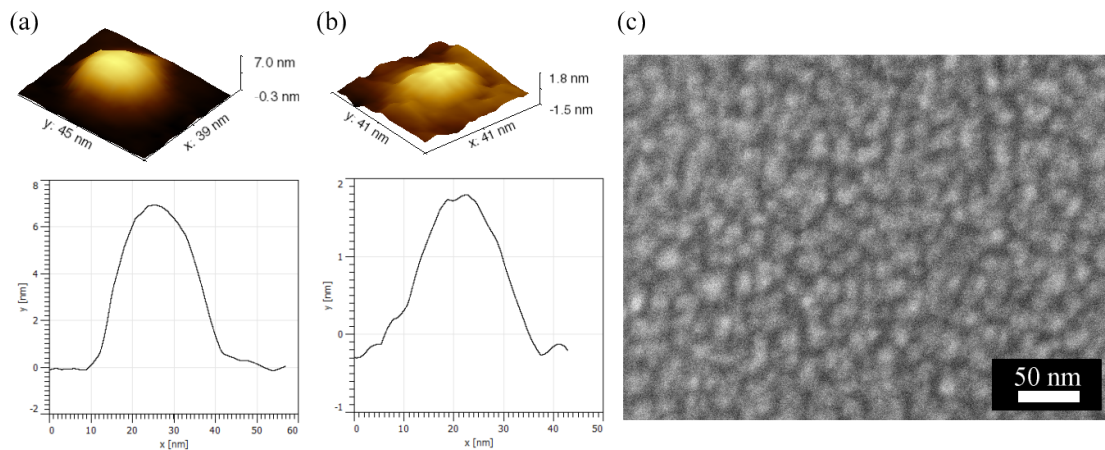
Figure 3.3: 3D views and line profiles of the AFM of one dot on the film of effective thickness of (a) 18 Å (12.9 ML), and (b) 22 Å (15.7 ML). (c) SEM scan of the germanium films with effective thickness of 22 Å (15.7 ML).

3.2   Laser-Induced Formation of Germanium Quantum Dots

In the second part of the experiment, we try to irradiate the control beam on the grown germanium film on silicon substrate. With varied shot numbers of control beam and effective thickness of germanium film, we try to find out a way to control the base diameter and the density of germanium quantum dots. The parameters of the growth of germanium film are the same as in Section 3.1 with fixed substrate temperature of 400 °C.

The fixed parameters of control beam are as follows:

- On-target beam size of control beam: 8.38 mm in clear aperture.

- Incident angle of ablation beam to target: $0°$.

- Air pressure during deposition $\sim 10^{-5}$ to 10^{-4} torr.

- The fluence of the control beam will be discussed later.

Since the beam profile of the control beam might affects the morphology of irradiated germanium films, we check the beam profile and make sure that it doesn't change in every experiment. Figure 3.4 is the beam profile of control beam shot by CCD and its contour graph.

(a)　　　　　　　　　　　　(b)
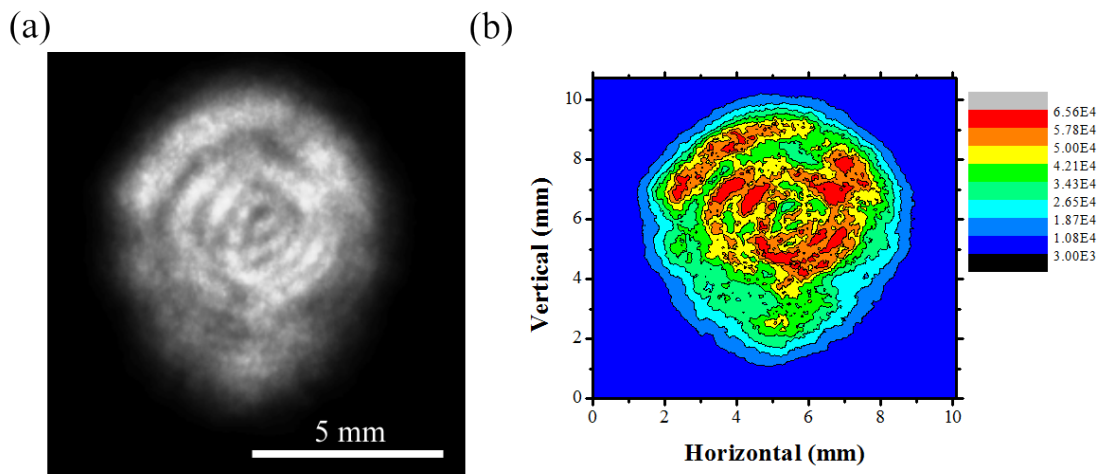
Figure 3.4: (a) CCD image of the beam profile of control beam. (b) Contour graph of the beam profile.

3.2.1 Effect of Control Beam Fluence

After irradiation on the germanium film with thickness of 2 Å (1.4 ML) with 20000 laser shots, the Figure 3.5 (b) shows the optical microscope image from one of the irradiated region and the corresponding region in the beam profile is shown in 3.5 (a). We found out that the average fluence of the region is about 60 mJ/cm^2. Here, we saw laser-induced

(a) **(b)**

(c)
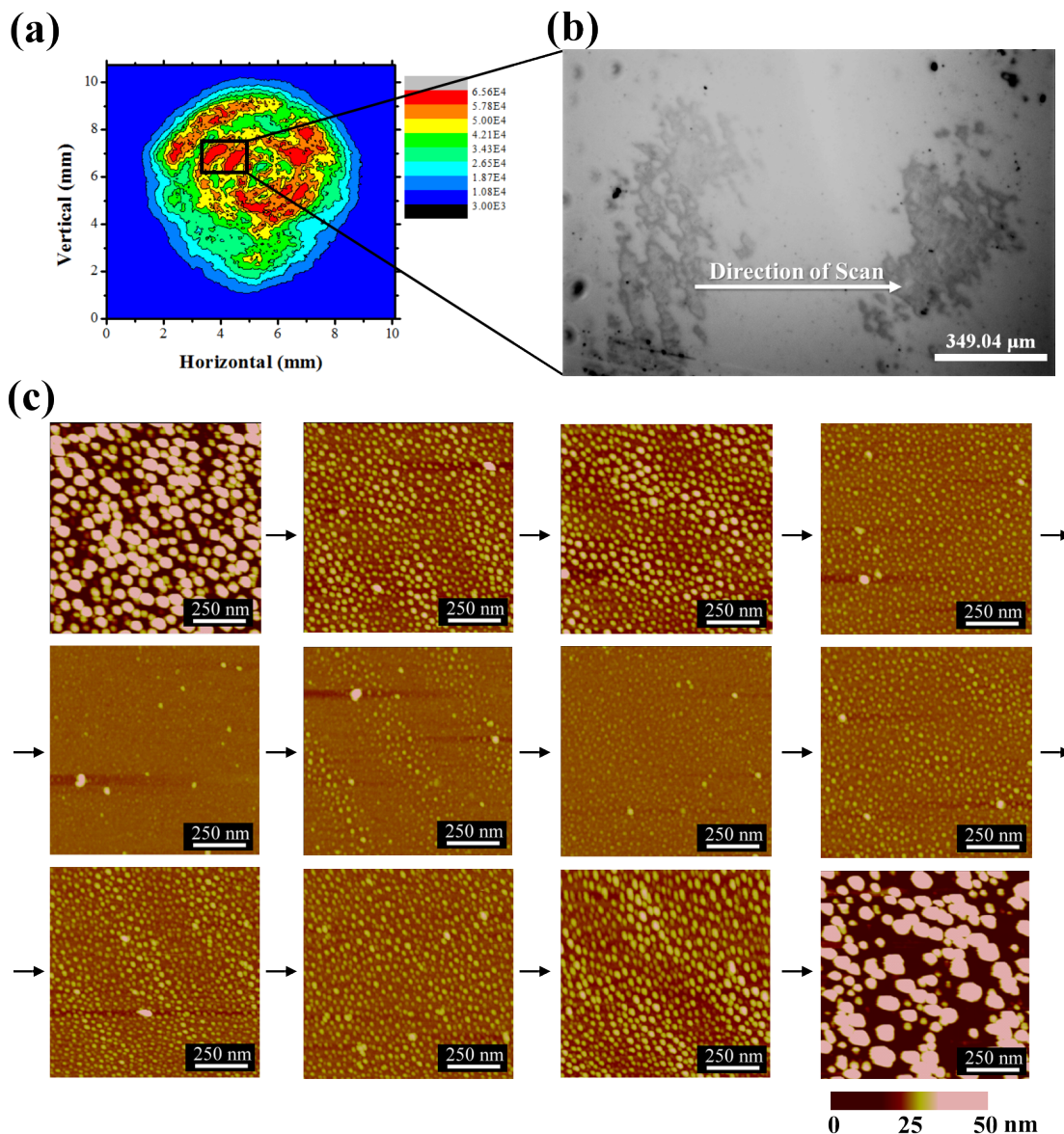
Figure 3.5: (a) Contour graph of the control beam profile and (b) the corresponding irradiated region of germanium film with thickness of 2 Å (1.4 ML) in optical microscope image after irradiation of 20000 laser shots. (c) AFM images of various regions in the line of the scan direction.

dots formation in this region from the AFM images. Then we scanned several AFM images on the scan line shown in Figure 3.5 (b), from the high fluence region (dark region) to another high fluence region. The AFM images is shown in Figure 3.5 (c). The distance between every images is about 50 μm. The 3D view of AFM images of Figure 3.5 (c) is shown in Figure 3.6. As we see in the AFM images, on the left dark region, the base diameter of dots are about 80 nm and height are about 68 nm. When we leave the dark region, the dots become smaller with the base diameter about 32 nm and height about 8 nm. In the middle of two dark regions, the dots are the smallest with base diameter about 20 nm and height about 1.2 nm. The variation of the size of dots on the right-half side is almost the same.

This variation of dots size could be as a result of the control beam fluence. However, no matter how we tuned the average fluence of a region of beam profile to 60 mJ/cm^2, we can only see dot formation near the dark region with the optical microscope. Thus
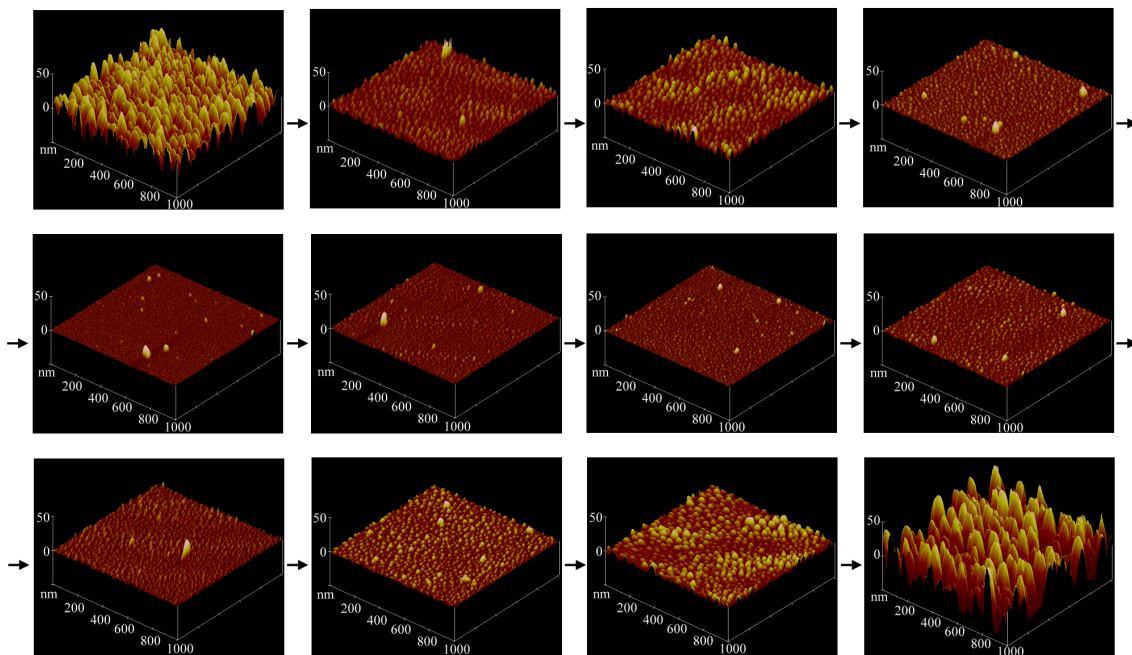
Figure 3.6: 3D view of AFM images of Figure 3.5 (b).

the laser-induced formation of dots might be as the result of the additional strain from the gradient of the high fluence laser irradiated region and the low fluence laser irradiated region as shown in Figure 3.7. The lattice parameters of both germanium and silicon are different with laser irradiation of different fluence. Thus the gradient of different lattice parameters in different region might cause the formation of dots.
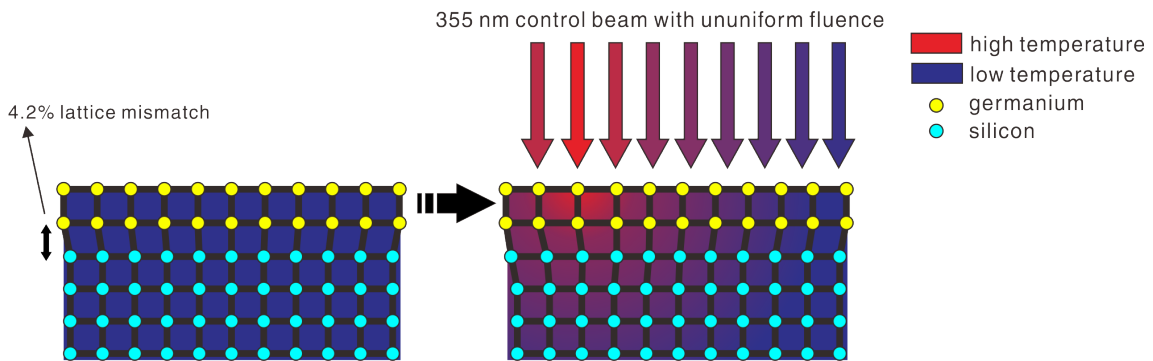
Figure 3.7: Schematic mechanism of the laser-induced formation of the quantum dots.

For the reason that the size of the dots changes from region to region near the dark irradiated region, we can only scan the same region in every sample with different parameters. Thanks to the grid lines on the samples shown in Section 2.2.5 and the substrate holder with two motorized linear translation stages in different direction mentioned in Section 2.3.2, we can make the control beam irradiated on the samples more precisely and find the dark region easily. In all our samples, we scan near the dark region to be sure the irradiation of the fluence gradient is the same.

3.2.2 Films of Various Shot Numbers of Control Beam

To figure out the formation process of the laser-induced dots, we irradiated the control beam on germanium film with thickness of 9 Å (6.4 ML) with various laser shot numbers and the same average fluence of 60 mJ/cm^2 in a region.

The result is shown in Figure 3.8. In the sample of irradiation with 200 shots, we

can observe the formation of structures of height about 3 nm, which are connected to each other. In the image of 1000 shots, the connections between the structures disappear and islands of height about 8 nm form. When the shot number comes to 10000 shots, the dots become smaller and higher with height of 13 nm. And then some of the dots gathered to be a bigger dots with height of 15 nm on the sample with shot numbeer 20000 shots. The mechanism of the process of the laser-induced formation is unclear and all of these were observed only in small region of several tens of micrometers. More mechanisms are needed to understand this phenomena.

Figure 3.8: 2D and 3D AFM images of irradiated germanium film with thickness of 9 Å (6.4 ML). The laser shot numbers are (a) 200 shots, (b) 1000 shots, (c) 10000 shots, and (d) 20000 shots, respectively.
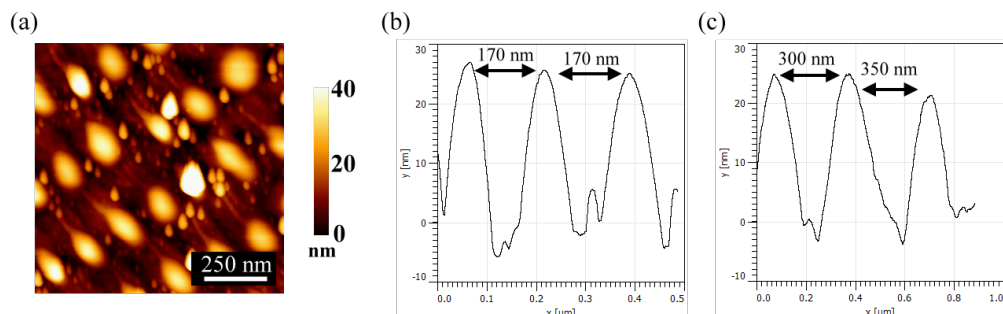
Figure 3.9: (a) AFM images of irradiated germanium film with thickness of of 9 Å (6.4 ML). The laser shot numbers is 40000 shots. (b) Line profile of the ordered dots from lower left to upper right, and (c) from lower right to upper left.
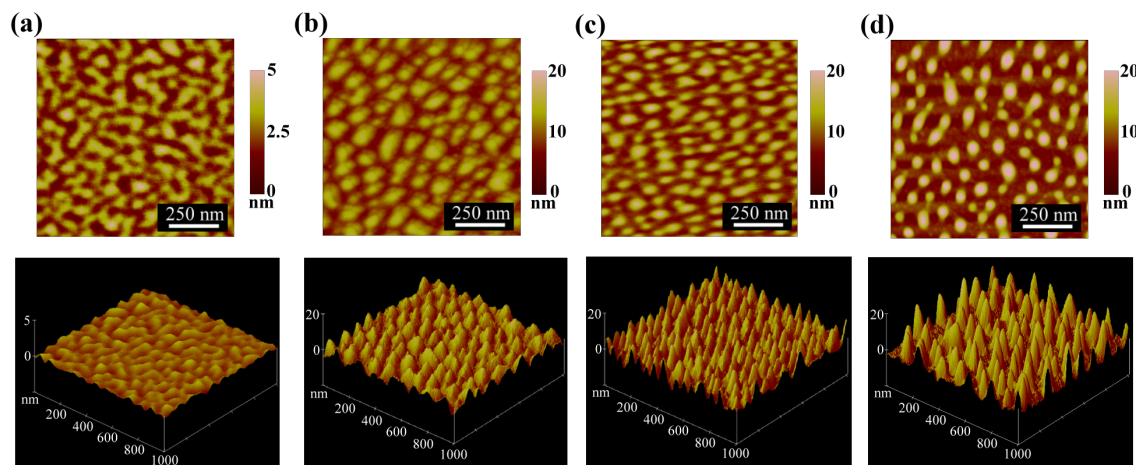
When it comes to 40000 shots, we see from Figure 3.9 (a) that the dots become larger with base diameter of 200 nm and height of 30 nm. The dots ordered in two directions are surprisingly observed. Figure 3.9 (b) and (c) shows the beam profile of the ordered dots from lower left to upper right and lower right to upper right, respectively. We found that in the direction of lower right to upper right, the distances between the dots are near to our wavelength of control beam, which is 355 nm. It indicates that it is due to the interference between the incident beam and the surface scattered wave as shown in Section 1.4.3.
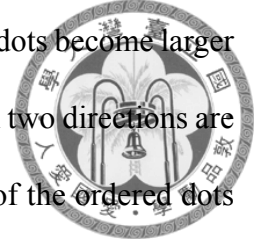
3.2.3   Films of Various Effective Thickness

With the same average fluence of 60 mJ/cm^2 in a region, we irradiate laser with 20000 shots on samples with various germanium film thickness. The result of 2D and 3D view of AFM images are shown in Figure 3.10 and the 3D view of AFM images of one dot and their line profiles are shown in Figure 3.11. The base diameter of these films with thickness of 2 Å (1.4 ML), 9 Å (6.4 ML), 14 Å (10.0 ML), and 18 Å (12.9 ML) are about 14 nm, 90 nm, 170 nm, and 360 nm, respectively. And the height is 1.3 nm, 15 nm,
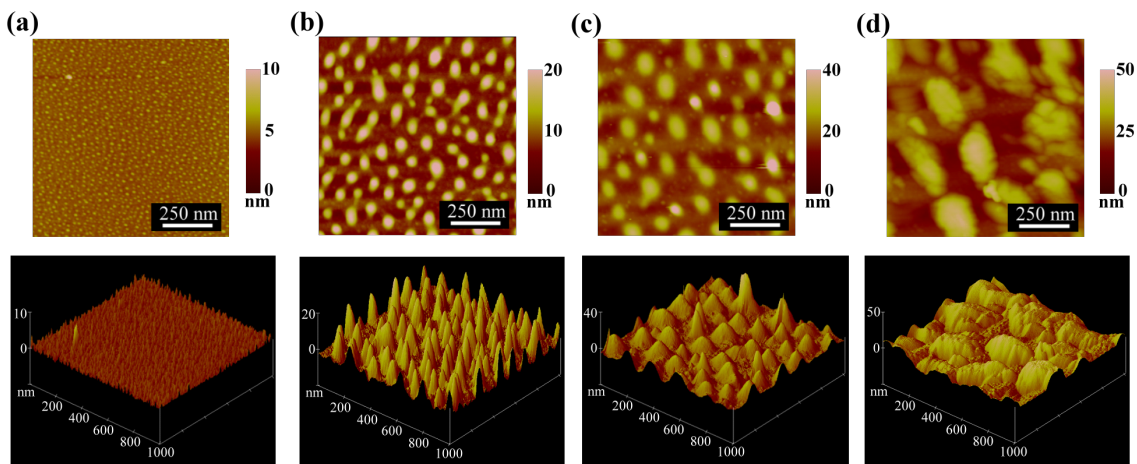
Figure 3.10: 2D and 3D AFM images of irradiation with 20000 laser shots on germanium film with thickness of (a) 2 Å (1.4 ML), (b) 9 Å (6.4 ML), (c) 14 Å (10.0 ML), and (d) 18 Å (12.9 ML).

16 nm, and 27 nm, respectively. We can see that both base diameter and height increases with the larger thickness of film. However, increment of base diameter is much more than that of height. The reason of this phenomenon might be that the thicker germanium film provides more materials for the dot formation. And the base diameter increases much more because the strain is stronger along the direction of the silicon surface due to the 4.2% lattice mismatch between silicon substrate and germanium film.
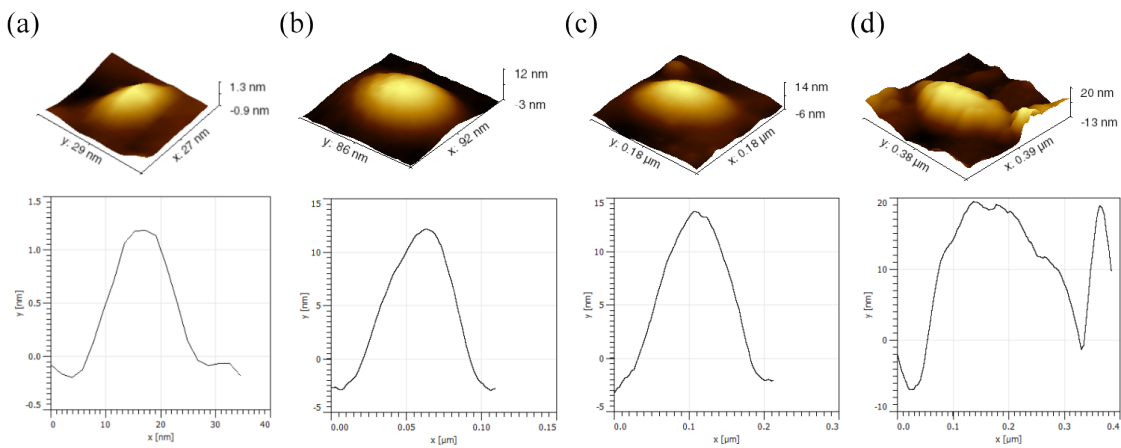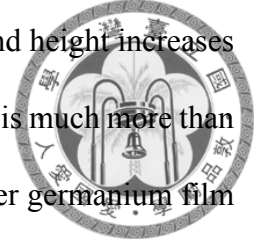
Figure 3.11: 3D AFM images of one dot and their line profiles of irradiation with 20000 laser shots on germanium film with thickness of (a) 2 Å (1.4 ML), (b) 9 Å (6.4 ML), (c) 14 Å (10.0 ML), and (d) 18 Å (12.9 ML).
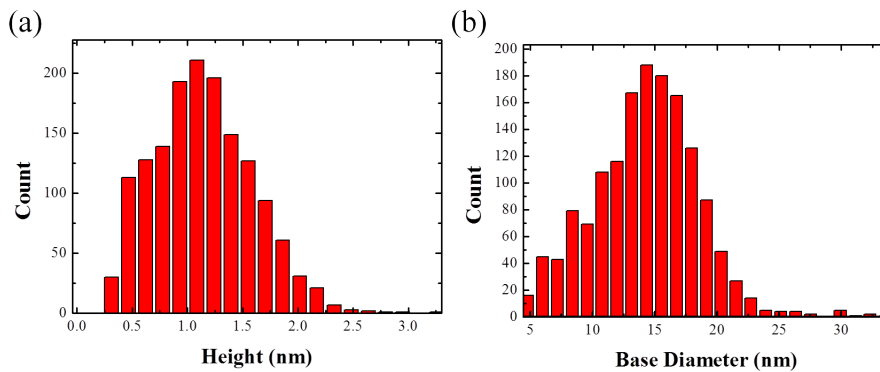
Figure 3.12: (a) The histogram of the base diameter and (b) the height of Figure 3.11 (a).

With the film thickness of 2 Å (1.4 ML), we got the highest density of dots, which is 1.6×10^{11} cm^{-2}. And we also saw the smallest dot of height of about 1.3 nm and base diameter of about 14 nm among our experiments. The histogram of base diameter and the height are shown in Figure 3.12 (a) and (b), respectively. Although the sheet density and

the mean dot size do not reach what we have seen in Section 1.3.1, we develop a new way to make quantum dots formation. Once we understand the mechanism of this phenomena, maybe we could control the density and size of the quantum dots. There are big potentials to make the smaller and more concentrated quantum dots.

Chapter 4

Summary and Future Prospective

We found out a new way to control the formation of germanium on silicon self-assembled QDs. By laser irradiation, we can see the laser-induced formation of dots under the critical thickness of spontaneous S-K mode growth. What's more, the larger the thickness is, the larger the base diameter and height of the dots are. That is, we can control the size of the quantum dots by varying thickness of the germanium film. In this way, the smallest average base diameter of about 17 nm and the density of dots of 1.6×10^{11} cm^2 are reached. Although both of them do not exceed the achievement from other works, there are great potentials to make them smaller and denser after we understand the mechanisms of this new method of quantum-dots formation. However, the restriction of the beam profile of control beam make it hard to form a sufficient large region with such small and dense quantum dots.

Since we believe that the laser-induced formation of the quantum dots is as result of the gradient of the fluence, we are planning to make the control beam split into two beams and interfere each other on the sample as shown in Figure 4.1 (a). On the interference patterns, there are full of gradient of fluence. By slightly moving the position of mirror of the split beam, the large fluence part of the interference fringe will irradiate averagely

on the whole region (Figure 4.1 (b)). Therefore, we can make the whole irradiated region

full of uniform quantum dots.
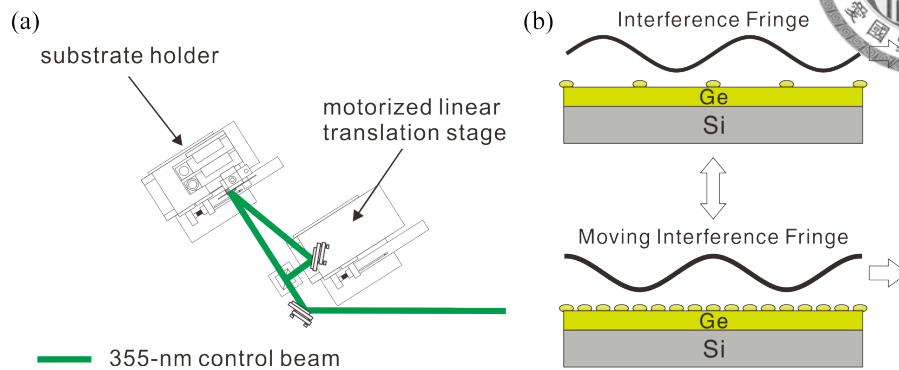
Figure 4.1: (a) Schematic setup of the interference of split control beams on the sample. (b) Interference fringe moveing back and forth to make whole plan full of quantum dots.

As seen in Figure 2.18, the optical absorption of germanium is about 40 times higher

than that of silicon at wavelength of 532 nm. Thus in our future work, we're also planning

to switch the wavelength of control beam from 355 nm to 532 nm. The beam will be

absorbed by the germanium film only, providing the direct heating on germanium film and

not on the silicon substrate [19]. Maybe it will help us to find out the mechanism of this

interesting process of laser-induced formation of germanium quantum dots (Figure 4.2).
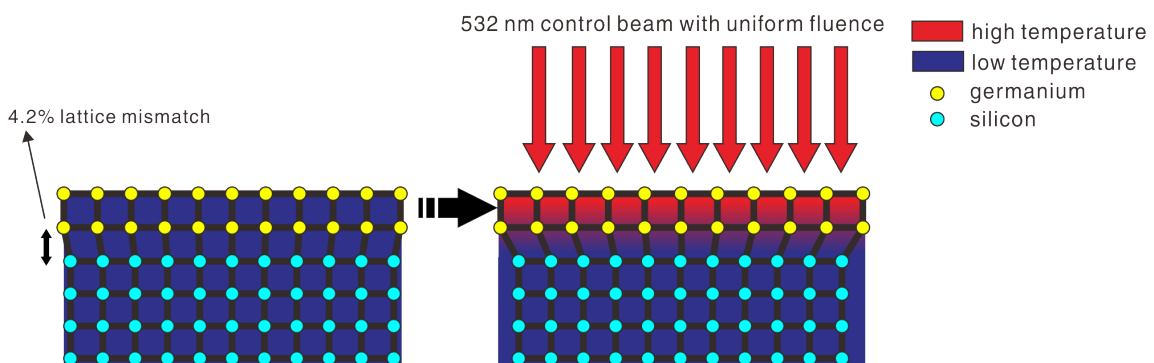
Figure 4.2: Schematic mechanism of the laser-induced formation of the quantum dots. In this graph the absorption of silicon is very small relatively to the absorption of germanium for light with wavelength of 355 nm.

References

[1] Mitsuru Sugawara. *Self-Assembled InGaAs/GaAs Quantum Dots*. Academic Press, 1999.

[2] Rudolf Bratschitsch and Alfred Leitenstorfer. Quantum dots: Artificial atoms for quantum optics. *Nature Materials*, 5:855--856, 2006.

[3] M. S. Hegazy and H. E. Elsayed-Ali. Growth of Ge quantum dots on Si(100)(2×1) by pulsed laser deposition. *Journal of Applied Physics*, 99:054308, 2006.
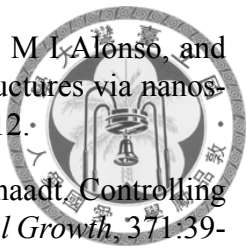
[4] I. Kamiya, Ichiro Tanaka, and H. Sakaki. Control of size and density of self-assembled InAs dots on (0 0 1)GaAs and the dot size dependent capping process. *Journal of Crystal Growth*, 201-202:1146--1149, 1999.

[5] Y. R. Li, Z. Liang, Y. Zhang, J. Zhu, S. W. Jiang, and X. H. Wei. Growth modes transition induced by strain relaxation in epitaxial MgO thin films on SrTiO$_3$ (001) substrates. *Thin Solid Films*, 489:245--250, 2005.

[6] D. J. Eaglesham and M. Cerullo. Dislocation-free Sranski-Krastanow growth of Ge on Si(100). *Physical Review Letters*, 64:1943--1946, 1990.

[7] J. L. Liu, S. Tong, and K. L. Wang. *Handbook of Semiconductor Nanostructures and Nanodevices*. American Scientific, 2005.

[8] J. L. Huang. Feasibility study of the control of the size distribution of Ge/Si quantum dots grown with pulsed laser deposition by laser pre-processing of the substrate. Master's thesis, National Central University, Taiwan, 2013.

[9] Kang L. Wang, Fellow IEEE, Dongho Cha, Jinlin Liu, and Christopher Chen. Ge/Si self-assembled quantum dots and their optoelectronic device applications. *Proceedings of IEEE*, 95:1866--1883, 2007.

[10] C. Teichert, M. G. Lagally, L. J. Peticolas, J. C. Bean, and J. Tersoff. Stress-induced self-organization of nanoscale structures in SiGe/Si multilayer films. *Physical Review B*, 53:16334--16337, 1996.

[11] A. I. Yakimov, A. V. Dvurechenskii, A. I. Nikiforov, S. V. Chaoekovskii, and S. A. Tiis. Ge/Si photodiodes with embedded arrays of Ge quantum dots for the near infrared (1.3-1.5 μm) region. *Semiconductors*, 37:1383--1388, 2003.

[12] Zhi Liu, Tianwei Zhou, Leliang Li, Yuhua Zuo, Chao He, Chuanbo Li, Chunlai Xue, Buwen Cheng, and Qiming Wang. Ge/Si quantum dots thin film solar cells. *Applied Physics Letters*, 103:082101, 2013.

[13] J M MacLeod, C V Cojocaru, F Ratto, C Harnagea, A Bernardi, M I Alonso, and F Rosei. Modified Stranski-Krastanov growth in Ge/Si heterostructures via nanostenciled pulsed laser deposition. *Nanotechnology*, 23:065603, 2012.

[14] Mathieu Helfrich, Bernd Terhalle, Yasin Ekinci, and Daniel M. Schaadt. Controlling structural properties of positioned quantum dots. *Journal of Crystal Growth*, 371:39--44, 2013.

[15] M. Gherasimova, R. Hull, M. C. Reuter, and F. M. Ross. Pattern level assembly of ge quantum dots on si with focused ion beam templating. *Applied Physics Letters*, 93:023106, 2008.

[16] Amro Alkhatib and Ammar Nayfeh. A complete physical germanium-on silicon quantum dot self-assembly process. *Scientific Reports*, 3:2099, 2013.

[17] A. Pascale, I. Berbezier, A. Ronda, and P. C. Kelires. Self-assembly and ordering mechanisms of Ge islands on prepatterned Si(001). *Physical Review B*, 77:075311, 2008.

[18] S. Watanabe, Y. Yoshida, S. Kayashima, S. Yatsu, M. Kawai, and T. Kato. In situ observation of self-organizing nanodot formation under nanosecond-pulsed laser irradiation on Si surface. *Journal of Applied Physics*, 108:103510, 2010.

[19] A Pérez del Pino, E György, J Roqueta I C Marcus, and M I Alonso. Effects of pulsed laser radiation on epitaxial self-assembled Ge quantum dots grown on Si substrates. *Nanotechnology*, 22:295304, 2011.

[20] Michale N. R. Ashfold, Frederik Claeyssens, Gareth M. Fuge, and Simon J. Henley. Pulsed laser ablation and deposition of thin films. *Chemical Society Reviews*, 33:23--31, 2004.

[21] J. H. Chuei. Control of the crystallinity of carbon films grown with pulsed laser deposition by using another laser pulse for synchronous laser processing. Master's thesis, National Central University, Taiwan, 2013.

[22] S. T. Su. Using pulsed laser deposition for growing TiO_2 mesoporous films with structures optimized for increasing the efficiency of dye-sensitized solar cells. Master's thesis, National Chung cheng University, Taiwan, 2013.

[23] *PV Education - Absorption Coefficient (http:// pveducation.org/ pvcdrom/ pn-junction/absorption-coefficient)*.

[24] *Digital Instruments - Scanning Probe Microscopy Training Notebook*.

[25] *Nanosensors - Catalogue of PointProbe Plus Silicon -SPM-Probes*.

[26] *Museum of Science - Scanning Electron Microscope (http://legacy.mos.org/sln/SEM/)*.

[27] T. M. Burbaev, T. N. Zavaritskaya, N. N. Mel'nik V. A. Kurbatov, V. A. Tsvetkov, K. S. Zhuravlev, V. A. Markov, and A. I. Nikiforov. Optical properties of germanium monolayers on silicon. *Semiconductors*, 35:941--946, 2001.